ASSESSING AVAILABLE WOODY PLANT BIOMASS ON RANGELANDS WITH LIDAR AND MULTISPECTRAL REMOTE SENSING

A Thesis

by

NIAN-WEI KU

Submitted to the Office of Graduate Studies of
Texas A&M University
in partial fulfillment of the requirements for the degree of

MASTER OF SCIENCE

May 2011

Major Subject: Forestry

Assessing Available Woody Plant Biomass on Rangelands with Lidar and Multispectral Remote Sensing

ASSESSING AVAILABLE WOODY PLANT BIOMASS ON RANGELANDS WITH LIDAR AND MULTISPECTRAL REMOTE SENSING

A Thesis

by

NIAN-WEI KU

Submitted to the Office of Graduate Studies of
Texas A&M University
in partial fulfillment of the requirements for the degree of

MASTER OF SCIENCE

Approved by:

Chair of Committee,	Sorin C. Popescu
Committee Members,	R. James Ansley
	Humberto L. Perotto-Baldivieso
	Anthony M. Filippi
Head of Department,	Steven G. Whisenant

May 2011

Major Subject: Forestry

ABSTRACT

Assessing Available Woody Plant Biomass on Rangelands with Lidar and Multispectral Remote Sensing. (May 2011)

Nian-Wei Ku, B.S., National Chiayi University, Taiwan

Chair of Advisory Committee: Dr. Sorin C. Popescu

The majority of biofuels are produced from corn and grain. The drawback to these sources of biofuels is the vast amount of cultivated land needed to produce substantial amounts of biofuel, potentially increasing the price of food and livestock products. Mesquite trees, a type of woody plant, are a proven source of bioenergy feedstock found on semi-arid lands. The overall objectives of this study were to develop algorithms for determining woody plant biomass on rangelands in Texas at plot-level using terrestrial lidar and at the local scale by integrating reference biomass and multispectral imagery.

Terrestrial lidar offers a more efficient method for estimating biomass than traditional field measurements. Variables from the terrestrial lidar point cloud were compared to ground measurements of biomass to find a best fitting regression model. Two processing methods were investigated for analyzing the lidar point cloud data, namely: 1) percentile height statistics and 2) a height bin approach. Regression models were developed for variables obtained through each processing technique for estimating woody plant, aboveground biomass. Regression models were able to explain 81% and

77% of the variance associated with the aboveground biomass using percentile height statistics and height bins, respectively. The aboveground biomass map was generated by using the cokriging interpolation method with NDVI and ground biomass data. According to cross-validation, ordinary cokriging estimated biomass accurately (R^2 = 0.99). The results of this study revealed that terrestrial lidar can be used to accurately and efficiently estimate the aboveground biomass of mesquite trees in a semi-arid environment at plot level. Moreover, spatial interpolation techniques proved useful in scaling up biomass estimates to local scale.

DEDICATION

To my parents and my brother

ACKNOWLEDGEMENTS

I sincerely appreciate my advisor, Dr. Sorin C. Popescu, for guiding me patiently and helpfully in my research and for supporting this study. I truly thank my committee, Dr. R. James Ansly, Dr. Humberto L. Perotto-Baldivieso, and Dr. Anthony M. Filippi, for their constructive comments and support. Special thanks to Dr. Ansley for the field survey assistance.

I am grateful to Dr. Mustafa Mirik, and my colleagues, Mr. Mark Karnauch, Mr. Ryan Sheridan, and Mr. Jared Stukey, for their contribution with the field survey. Thanks to Dr. Kaiguang Zhao and Dr. Muge Mutlu Agca for their worthy comments. Special thanks to Dr. Marian Eriksson for donating her time to help me with the data analysis.

I am thankful for my parents' and my younger brother's support. I would also like to thank Miss Zhauhui Chi for her help. Lastly, I offer my regards to all of those who assisted me with the completion of my thesis.

TABLE OF CONTENTS

Page

LIST OF FIGURES

Page

Page

LIST OF TABLES

1. INTRODUCTION AND LITERATURE REVIEW

More than 85% of energy consumed, including approximately two-thirds of electricity and the majority of transportation fuel in the United States (Department of Energy, 2010), is derived from fossil fuels. Fossil fuels are the result of organic material being under pressure millions of years and include coal, petroleum, and natural gas. After the industrial revolution, the demand for fossil fuels increased. As a result of the enormous demand for fossil fuels, the Earth's reserves of fossil fuels are decreasing dramatically. Therefore, people are searching for alternatives to fossil fuels to support the ever increasing energy demands.

Plants are increasingly being considered as a bioenergy source, including solid biomass, liquid fuels and various biogases (Demirbas, 2009). The majority of liquid biofuels are refined as ethanol from corn and grain. Statistically, around 8 billion gallons of ethanol were produced in the US in 2008 and required one-fifth of the 80 million acres dedicated to growing corn and an additional 27 million tons of grain (Clayton 2008). As such, a vast amount of corn and grain is utilized for producing ethanol rather than food products and livestock feed, potentially increasing the price of food products and livestock feed.

The encroachment of woody plants on rangelands and cultivated lands is a critical issue to land owners and scientists (Van Auken, 2000). Woody plant

---

This thesis follows the style of *Remote Sensing of Environment*.

encroachment directly threatens the grass forage production for livestock and reduces the area of cultivated lands. In Texas, an overwhelming amount of rangeland and grassland is infested with various species of woody plants because the mechanical and chemical treatments to reduce the amount and density of woody plants are becoming increasingly uneconomical (Brown and Archer, 1989). The rate of woody plant encroachment is increasing rapidly in the rangelands of the southwestern US.

Mesquite and other rangeland trees have been considered bioenergy feedstock (Felker 1984; Ansley et al., 2010). If mesquite trees can be removed from rangelands without significantly disturbing grasses and the bioenergy benefits can be obtained, the removal of woody plants can serve a dual-purpose: to mitigate the negative effects associated with woody plant encroachment and provide bioenergy feedstock.

In order to know the amount of bioenergy feedstock available from woody plants, the woody plant biomass has to be estimated. Trees normally have one basal stem for each root system (e.g., pine or oak), but rangeland woody plants generally have multiple basal stems for each root system (e.g., mesquite) (Figure 4). The conventional, manual measurements of tree height and individual basal stem diameter are used to calculate both woody plant and tree biomass; however, basal stem diameter is measured at 10 or 15.24 cm above ground for woody plants while tree basal stem diameter is measured at 1.4m (referred to as diameter at breast height (DBH)) (Chojnacky, 2002; Jenkins et al., 2003; Northup et al. 2005; Ansley et al., 2010). The conventional measurements are time-consuming, particularly measuring the stem diameter; thus, more

efficient measurement strategies, such as utilizing remote sensing, should be developed to estimate the biomass of woody plants over large forest and rangeland areas.

Lidar (Light Detection and Ranging) is an active remote sensing system that significantly differs from passive remote sensing systems in that it provides its own energy source instead of relying on energy reflected off of or radiated from the object under observation. Because of this, passive remote sensing cannot directly measure the terrain elevation and the height of objects, while lidar acquires three-dimensional information (Lefsky et al., 2002). Lidar remote sensing provides the capability to analyze woody plant structure at a high level of detail and the ability to estimate biomass more efficiently over the entire study extent.

Airborne lidar systems have been used for forest assessment since the 1980s (Nelson, 1988). Lidar creates a convenient and efficient approach for obtaining forest measurements. Recently, lidar data have been applied in a variety of forest and rangeland studies, such as deriving forest characteristics (Nelson, 1988; Popescu et al., 2003), forest biomass estimation (Lefsky et al., 1999; Popescu, 2007), forest structure analysis (Maltamo et al., 2005), carbon content estimation in forest (Patenaude et al., 2004), and identifying individual trees in rangelands (Chen et al., 2006).

Lidar systems can be mounted on a variety of platforms, such as satellites, aircraft, or terrestrial (both mobile and static). The majority of studies describe the use of lidar data collected from satellite and airborne platforms. In contrast, the use of terrestrial lidar systems, or terrestrial laser scanners, for forest and woody plant research accounts for only a small number of studies. Terrestrial lidar has demonstrated promise

as an objective and consistent forest assessment tool (Hopkinson et al., 2004). Terrestrial lidar has also developed rapidly in surveying as an efficient tool for fast and reliable three-dimensional data acquisition, giving merit to its potential for forest measurement. Methods for the automatic detection of trees in terrestrial lidar data as well as the automatic determination of diameter at breast height (DBH), tree height, and 3D stem profiles are outlined in Maas et al. (2008). Moreover, terrestrial lidar can capture detailed stem profiles of standing trees to derive accurate DBH and assess branch heights, where measurement of the branches near the base of the live crown and below it have excellent accuracy (Henning and Radtke, 2006a). Terrestrial lidar can also provide high-resolution and spatially-explicit assessments of plot-level forest canopy structure (Henning and Radtke, 2006b). Forest understories can be depicted much more accurately with terrestrial lidar than airborne lidar and other two-dimensional remote sensing technologies, such as aerial photographs or satellite imagery.

Vegetation indices are indicators used to analyze vegetation from spectral information collected by remote sensing system. In particular, the normalized difference vegetation index (NDVI) is commonly applied to measure regional vegetation patterns. Anderson et al. (1993) employed Landsat TM data to derive NDVI for semiarid rangeland and concluded that the green biomass and NDVI have a high degree of association. Anderson et al. (1993) also noted that when NDVI was combined with greenness strata, it was possible to predict green biomass levels using univariate regression models. Zheng et al. (2004) used Landsat ETM+ data to estimate aboveground biomass for pine forests and found a strong relationship between

aboveground biomass and the correct NDVI. Regional examples, such as those presented above, provide evidence that NDVI could be used to estimate aboveground biomass at a local scale.

Although terrestrial lidar has been applied in forest studies, many of these studies were in nursery conditions or using plastic trees indoors. Of those studies conducted in field conditions, most concentrated on forest structure analysis and deriving tree characteristics. Few lidar studies focused on rangeland woody plants. This study aims to develop a methodology for utilizing terrestrial lidar data to assess plot-level aboveground woody plant biomass by developing algorithms to estimate woody plant biomass and investigate the relationship to ground-measured biomass. In addition, the reference biomass data was combined with vegetation indices data to calculate woody plant biomass at a local level. This study addresses the following objectives:

1) Development of algorithms to determine aboveground woody plant biomass at plot level from terrestrial lidar data.
2) Investigate a synergistic approach that integrates terrestrial lidar data and multispectral imagery with geostatistics techniques to calculate aboveground woody plant biomass at the local scale.

2. METHODOLOGY AND MATERIALS

2.1 Study area

The study area is located at the northern limit of honey mesquite's range (Figure 1A), in the Texas AgriLife Research and Extension Center's Smith Walker Research Unit, outside of Vernon in Wilbarger County, Texas (Figure 1B). Wilbarger County is located on the Texas Rolling Plains, consisting of sandy, loam, and clay loams soils that support tall grasses, mesquite (Table 1.), and shinnery oak trees. Average annual precipitation is 25.65 inches, and temperatures range from an average minimum of 29˚F in January to an average maximum of 98˚F in July (TSHA 2010).

The Smith Walker Research Unit (34˚02' N, 99˚14' W) is approximately 223 hectares of cultivated land and 684 hectares of rangeland. The cultivated land is used predominantly for small grains and the forage crop research program. The rangelands are used for range animal nutrition programs and rangeland ecology and management programs. Terrestrial lidar data were collected in the rangeland area of the research unit.

The land cover in the Smith Walker Research Unit consists of grass, honey mesquite (regrowth, young, and old), bare soil, and water. Using the patch-corridor-matrix model from landscape ecology (Forman 1995) to describe the research unit, the matrix is grass with honey mesquite (*Prosopis glandulosa*) as the dominant patch. Honey mesquite is an introduced species that can reach 6 meters in height, averaging 3-4 meters within the study area, excluding regrowth. Patches of honey mesquite vary in

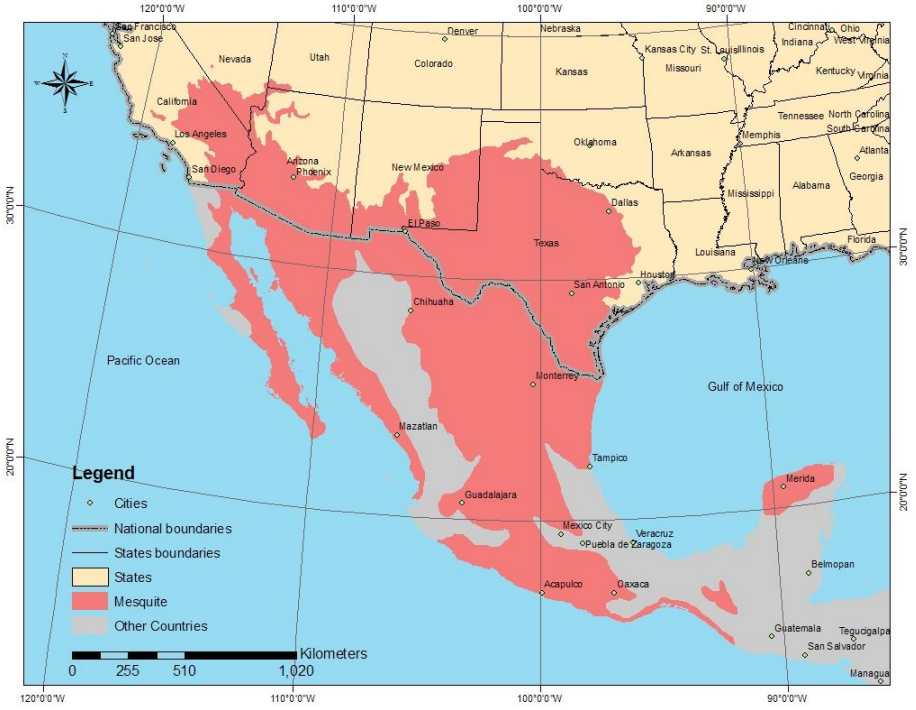

(A)

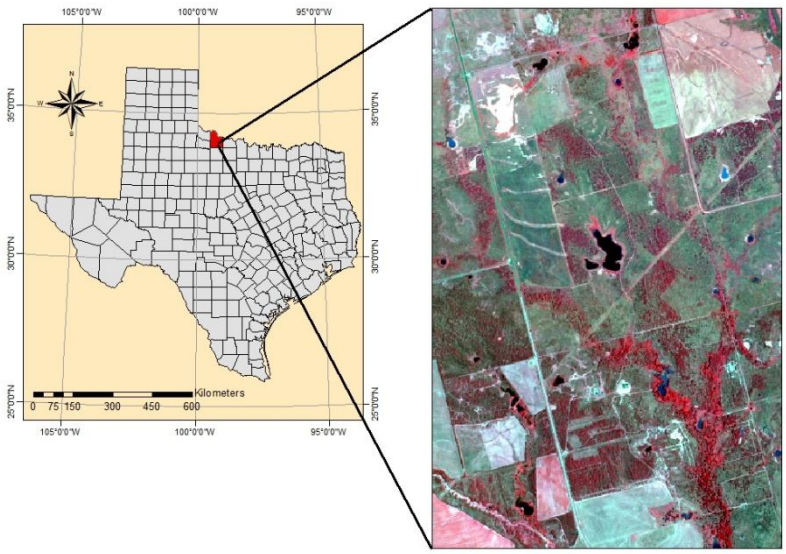

(B)

Figure 1. (A) Distribution map of mesquite trees in North America (Little, 1976). (B) The location of Smith Walker Research Unit, Vernon, Texas.

size, with small patches containing only one or two trees while large patches are comprised of hundreds of trees. The majority of the old mesquite trees are located in the northern portion of the study area where the young and new regrowth are found throughout.

Table 1. Honey mesquite characteristics (Little, 1980)

Height	~ 6 m
Diameter	~ 0.3 m
Leaves	Bipiinately compound 7.5 to 20 cm
Twigs	Slightly zigzag with stout, yellowish, mostly pared spines 0.6 to 2.5 cm
Flowers	6 mm long; stalkless, light yellow
Fruit	9 to 20 cm long; narrow pod; maturing in summer
Habitat	Sandy plain and sandhill; in short grass, desert grasslands, and deserts

Terrestrial lidar was used to scan 25 plots during the leaf-off season to reduce laser occlusion caused by leaves. Mesquite tree age is homogenous within each plot and ranges from regrowth to mature. Heights range between 1 and 6 m. The plots are distributed randomly in the Smith Walker Research Unit and are located on various soil types and are grouped according to mesquite tree age and soil type: (1) bottomland with mature mesquite; (2) deep clay loam upland with mature mesquite; (3) deep clay loam upland with regrowth mesquite; and (4) shallow upland with mature mesquite.

2.2 The terrestrial lidar system

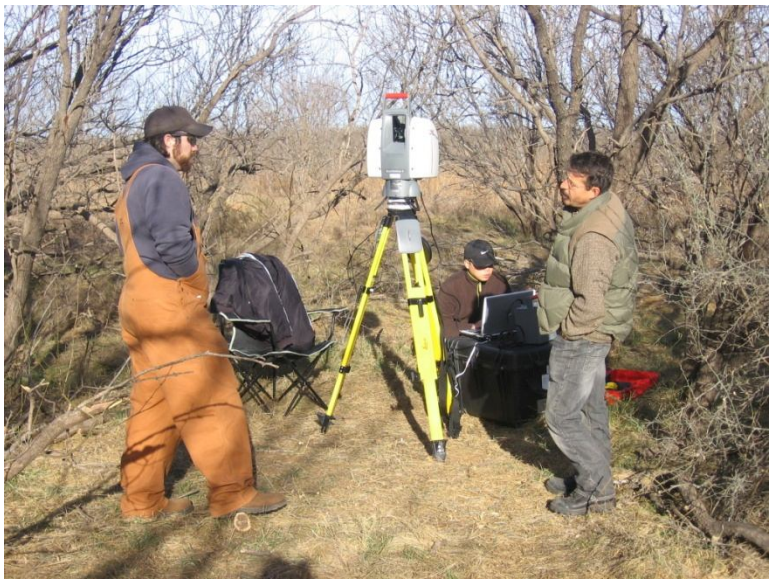

Figure 2. Terrestrial lidar system, Leica ScanStation2, in the field setting of this study.

The terrestrial lidar system, a Leica ScanStation 2 laser scanner, was designed for infrastructure surveys, topographic surveys of small sites, and for scanning buildings (Figure 2). The scanner is safe for field technicians, cuts initial survey costs, and reduces site re-visits. In addition, compared to other terrestrial lidar systems, the Leica ScanStation 2 has a higher pulsed scan frequency which significantly reduces the amount of time needed for field work. After completing the time-consuming, conventional measurements to obtain biomass estimates, the scanner was employed to collect point cloud data for each plot.

The Leica ScanStation 2 scanner uses a pulsed green laser (532 nm) with a maximum scan rate of 50,000 points/second with reported single point accuracies of

4mm for distance measurement and 6mm positional measurement from 1 to 50 m. The scanner has a range of 300 m for surfaces with 90% reflectivity, all with a small beam diameter. The laser scanning system provides a 360 degree horizontal and 270 degree vertical field of view, omitting only a small area on the ground, just below the scanner.

2.3 Field survey

The terrestrial lidar data were collected from 25 study plots in Smith Walker Research unit (Figure 3) in December 2008, March 2009, and December 2009, leaf-off season. The scan time for each plot ranged from 1.5 to 2 hours, with two separate scans completed at each plot. Due to battery constraints, the terrestrial lidar could not scan more than 4 plots per day. Although the terrestrial lidar is an active remote sensing system that can work in day time and night time conditions, the scanner cannot operate in the extremely cold or hot temperatures ($< 0^{\circ}C$ or $> 40^{\circ}C$) or during precipitation events. The resolution of terrestrial lidar data depends on the field of view and the range (or depth) parameter settings. In the study, the field of view was 140 degree in the horizontal direction and 100 degree in the vertical direction. The point spacing at 20 m from the scanner was 1.78x2.14 cm in the horizontal and vertical directions. Table 2 shows specific information for the lidar point data of each plot.

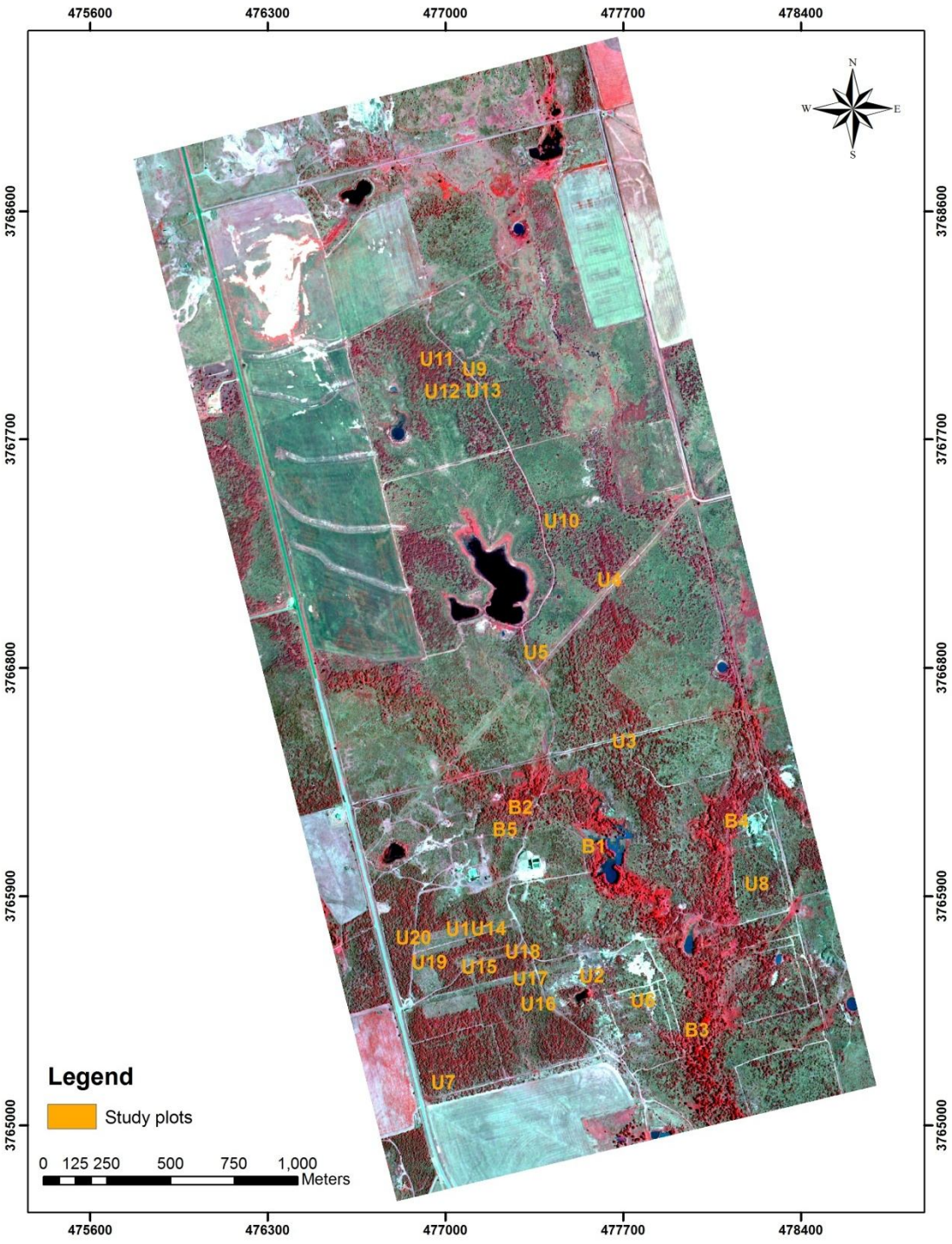

Figure 3. The locations of all study plots in Smith Walker Research Unit. Plot labels are displayed in orange.

Figure 4 Mesquite trees with multiple stems on the study plot (Plot U16).

Figure 5. Scattered mesquite trees in a study plot (Plot U20) and a target (red) used for merging the two scans of a plot from opposite directions. The white PVC pipes were used to mark the boundary of a study plot.

Each study plot measured 5 m wide by 20 m long and contained honey mesquite of similar age and height (Figure 5). The dimensions of the plots were designed to efficiently estimate standing mesquite tree biomass based on basal stem diameters, both manually and using the scanner. A larger plot would have been time-consuming to measure and a smaller plot would have been too small to contain trees of average size for the area. The terrestrial lidar scanner was positioned along one of the long-boundaries of the plot for the first scan and then moved to the opposite side for the second scan. The two stationary targets were positioned near the short boundaries of the plot (Figure 6). The arrangement of the terrestrial lidar scanner and the targets can be modified so the targets can clearly be scanned from both scanner locations without being moved. The two targets served as reference points in each lidar point cloud, which allowed them to be seamlessly merged into a single three-dimensional model using the Leica Cyclone software package, which is also used to run the scanner in the field. Table 2 shows the lidar point cloud data of each study plot.

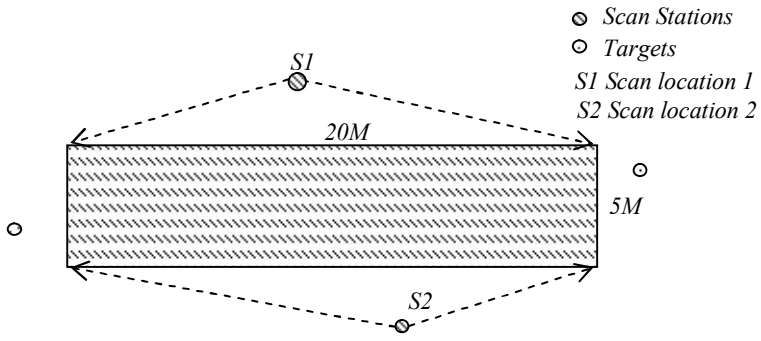

Figure 6. A conceptual diagram of the arrangement of the terrestrial lidar and targets for a plot. The dashed arrows indicate the angular extents of the scans.

Table 2. The lidar point cloud data of each plot

Plot ID	Points Density (points/m^3)*	Mean Height (m)	Standard Deviation	Max Height (m)
B3	314	1.47	1.40	5.72
B4	943	1.12	1.26	5.87
B5	1643	0.84	1.01	4.29
D1	1486	0.34	0.62	3.90
D2	314	1.90	1.80	6.73
M13	157	2.04	1.81	6.53
M3	871	1.27	1.30	5.69
M6	1014	0.91	1.30	5.93
S4	1557	0.64	0.71	3.64
S6	1243	0.53	0.56	3.03
U10	1043	2.11	1.66	5.73
U14	1171	1.64	1.60	6.50
U15	1271	1.72	1.67	6.31
U16	886	1.23	1.20	4.74
U17	1200	1.34	1.25	5
U18	1071	1.77	1.60	6.56
U19	1257	0.39	0.56	2.90
U20	1114	0.50	0.58	3.11
U21	757	1.28	1.03	4.25
U22	1471	0.32	0.35	2.18
U23	857	0.45	0.45	2.12
U3	929	0.94	1.15	4.70
U5	1886	0.41	0.68	3.15
U7	714	0.95	1.19	5.42
U8	1571	1.05	1.10	4.33

* The height of computing the point density is assumed 7 m and the base area is the plot size.

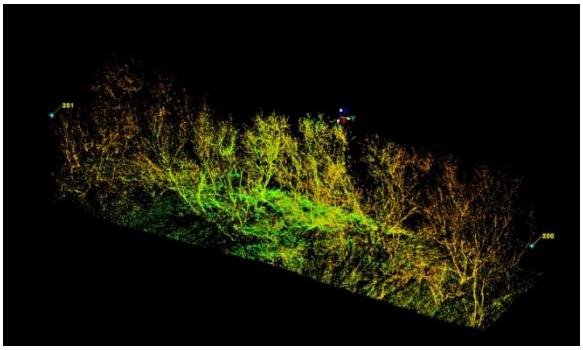

(A)

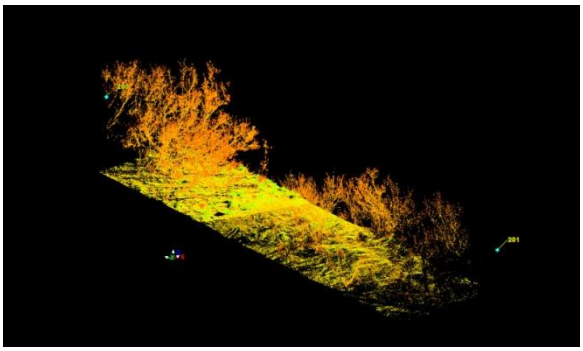

(B)

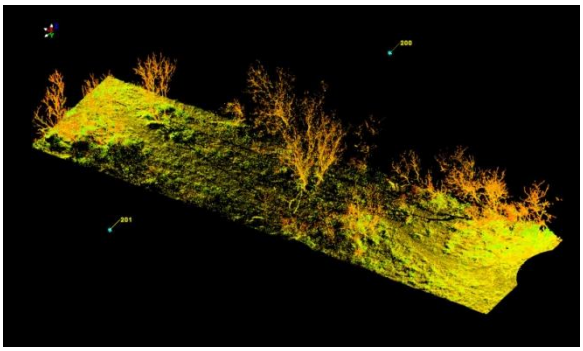

(C)

Figure 7. (A) Dense (Plot B3) (B) moderate (Plot M3) (C) thin (Plot D1) mesquite tree study plot.

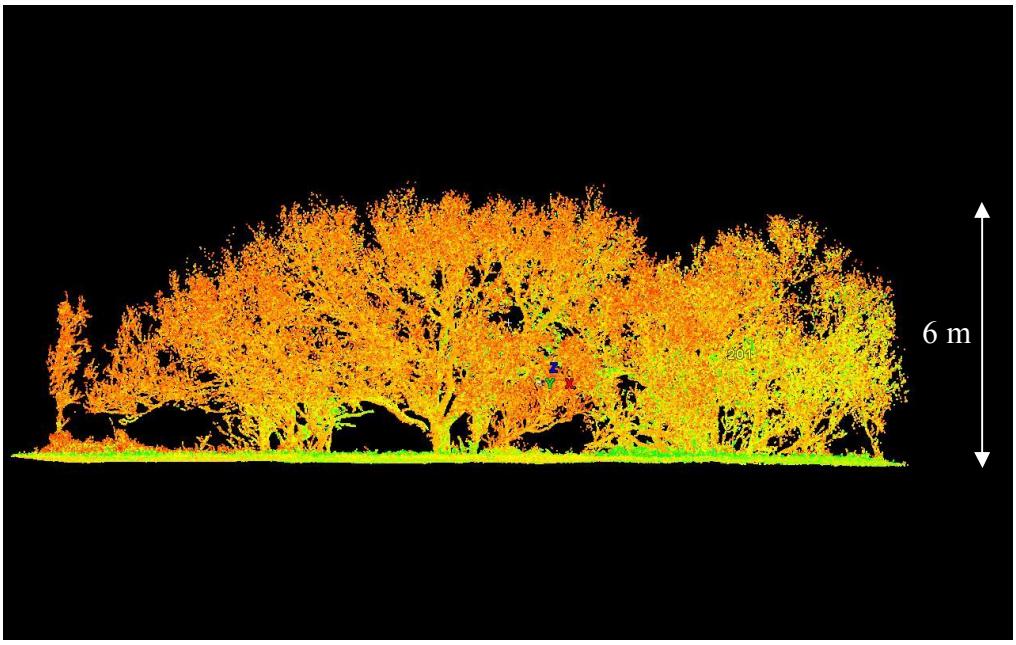

(A)

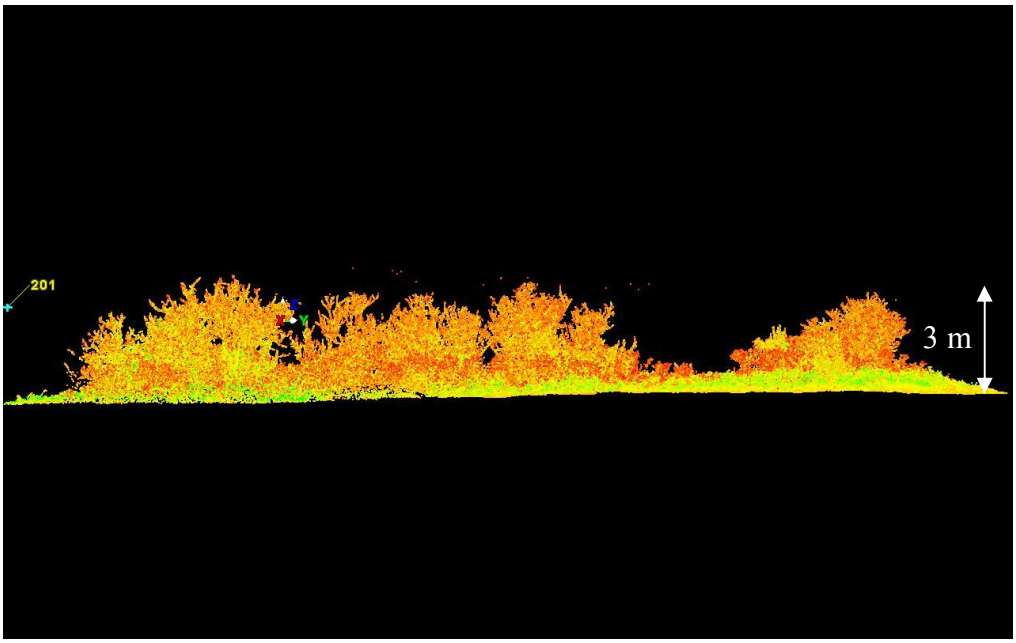

(B)

Figure 8. An example of mesquite tree height variation between plots (A) 6 m height (Plot M13) (B) 3 m height (Plot S6).

2.4 Reference data for aboveground biomass

The manual measurements of stem diameters for the aboveground biomass reference data were collected during the same time period as the laser scans. The manual estimates of tree biomass in each plot included the measurement of diameter of each basal stem in each scanned plot between 5 and 15 cm above ground.

The total aboveground biomass of each stem was estimated using the allometric equation (eq. 1) developed by Ansley et al. (2010), based on the relationship between oven dried (OD) plant biomass and basal stem diameter. Regression showed a high correlation (R^2 =0.97). Biomass of all stems was summed to determine biomass per plot. Biomass estimates were then extrapolated from the 100 square meter plot area to one hectare.

$$Y=0.0175x^{2.831} \qquad \text{(eq. 1)}$$

Y: Oven dried (OD) plant biomass (kg)

x: Stem diameter (cm)

2.5 Lidar point cloud data processing

The lidar point cloud data were processed using Leica Cyclone and Quick Terrain Modeler (QTM) software, before the point cloud data were analyzed. Cyclone provided the complete set of tools for merging the point clouds captured from different scanner positions at each plot. QTM is a three-dimensional point cloud and terrain visualization software package developed by John Hopkins University's Applied Imagery Lab. The Above Ground Level (AGL) analysis tool in QTM was used to calculate the relative height of the points above the ground.

Since the scanning process resulted in two point clouds for each plot, the first step for processing the data was to merge the two point clouds using Cyclone (Figure 9). The process created a single point cloud containing data from both scanner locations. Next, the points located in the 5m x 20m rectangular plot were extracted from the initial three-dimensional model in order to correlate them with the reference biomass data. This three-dimensional point cloud was compared with aerial photos and the GPS-generated shapefiles to identify the scanned plot. The plot boundaries were easily identified in the

point cloud using four PVC pipes positioned at the corners of each plot. Next, a boundary was created using Cyclone's fence tool and the points outside of the plot were removed. After selecting and extracting the scanned plot, the next step was to remove non-natural points visible within the plot, such as the reference targets and PVC pipes. In the end, a point cloud of the scanned plot was generated.

After the plot was extracted using Cyclone, each point cloud was exported to an ASCII file and imported into Quick Terrain Modeler. The AGL analysis tool calculated and assigned an elevation value by estimating a height to the ground surface for every point in the point cloud. Heights assigned to points by the AGL analysis can be used as criteria for selective removal of non-useful vegetation and canopy information from a point cloud allowing users to clearly see and identify objects under foliage or other obstructions. The ground points were removed to produce an initial vegetation height model.

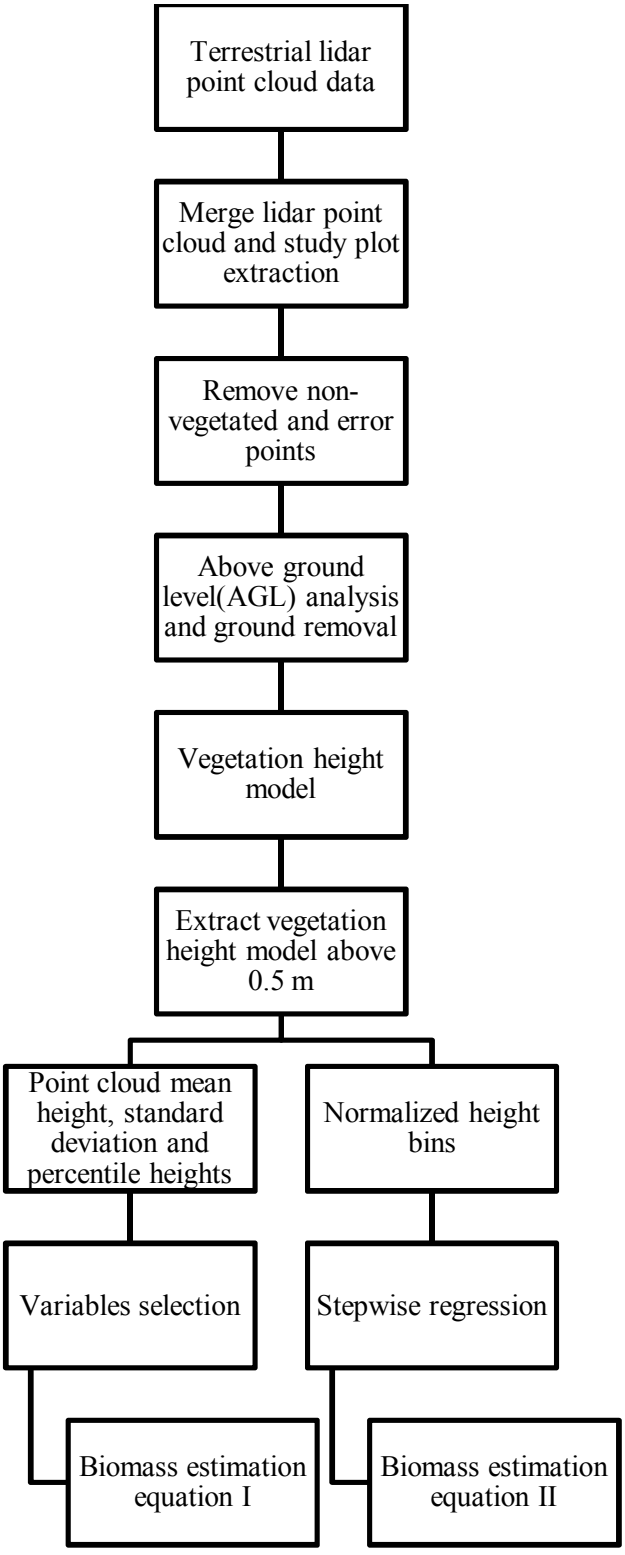

Figure 9. Flow chart of lidar point cloud data processing.

2.6 Lidar point cloud data analysis

In order to derive independent variables needed for the regression models of woody plant biomass estimation, the point cloud data were analyzed in two approaches. The first approach used the mean height, standard deviation and percentile heights as independent variables for the regression model. Magnussen and Boudewyn (1998), Næsset and Bjerknes (2001), and Næsset (2004) used a similar approach with airborne lidar for estimating tree height measurements, tree crown properties, and forest stand inventory parameters.

The mean height, standard deviation and percentile heights of lidar point cloud data were calculated from points in the vegetation height mode with heights above 0.5 m (VHM5) for each plot. Points below 0.5 m may result from laser shots hitting the ground and grass (Figure 10). VHM5 reduced the influence of low lying vegetation, ground, and rocks.

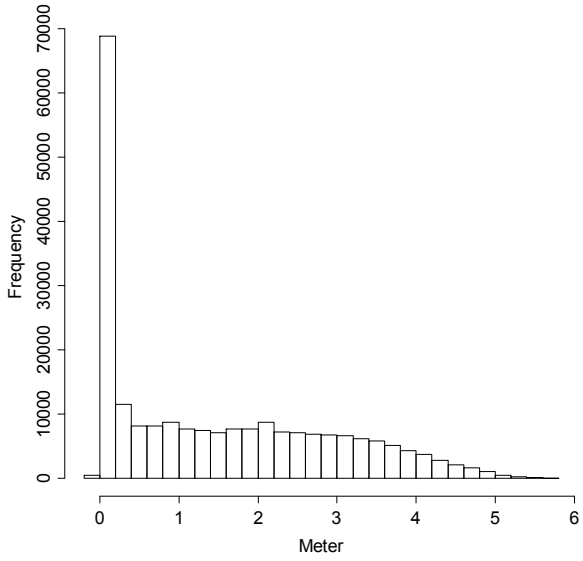

(a)

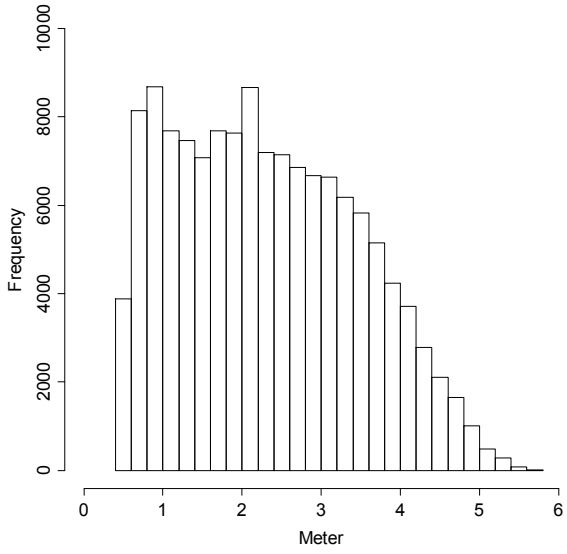

(b)

Figure 10. The distribution of point cloud data in the vegetation height model and the distribution of point cloud data in the vegetation height model above 0.5 m for a single plot. (Plot B3)

The 25th, 50th, 75th, 90th, and 95th percentile height and Maximum height were computed from VHM5 (Table 3). Mean height, standard deviation, and each percentile of vegetation height model were individually compared to the biomass reference data to build the regression relationships. Statistics extracted from VHM5 were compared to ground biomass reference data to establish a correlation.

The second approach used lidar height bins (Popescu and Zhao, 2008). Generally, lidar height bins represent layers or slices of point cloud data at vertical height intervals above ground (Figure 11). The height bins are essentially conventional, multiband, two-dimensional representations of lidar-derived voxels, or volumetric pixels, as they contain the frequency of laser returns within a three-dimensional space.

The normalized height bins were also extracted from VHM5. The first height bin contained points between 0.5 m and 1 m and the rest of the height bins are at 1 m intervals (i.e., 1-2m, 2-3m, etc.) (Figure 12). The last height bin contained points with heights greater than 6 m. Next, all height bins were divided by the total amount of laser points above 0.5 m to normalize the data and eliminate the effect of varied point density throughout the plots, resulting in seven normalized height bins to build another new biomass equation from.

Table 3. The list of variables

Variables of Lidar metrics	Description
Standard deviation, mean and percentile heights	
Mean_h	The mean height
Std_h	The standard deviation
Per25_h	25 percentile height
Per50_h	50 percentile height
Per75_h	75 percentile height
Per90_h	90 percentile height
Per95_h	95 percentile height
Max_h	Maximum (100 percentile) height
Height Bins	
NHbin1	Normalized height bins from 0.5 m to 1 m
NHbin2	Normalized height bins from 1 m to 2 m
NHbin3	Normalized height bins from 2 m to 3 m
NHbin4	Normalized height bins from 3 m to 4 m
NHbin5	Normalized height bins from 4 m to 5 m
NHbin6	Normalized height bins from 5 m to 6 m
NHbin7	Normalized height bins greater than 6 m

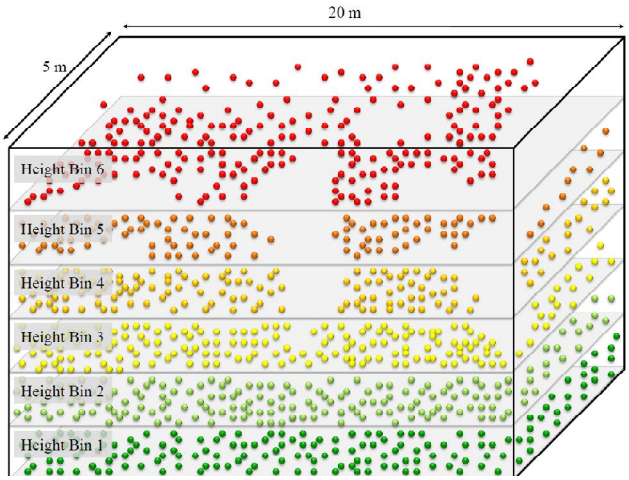

Figure 11. The concept of height bins in a study plot. The interval between height bins is user-defined height (Table 3). Points are colored based on the height bin they belong to.

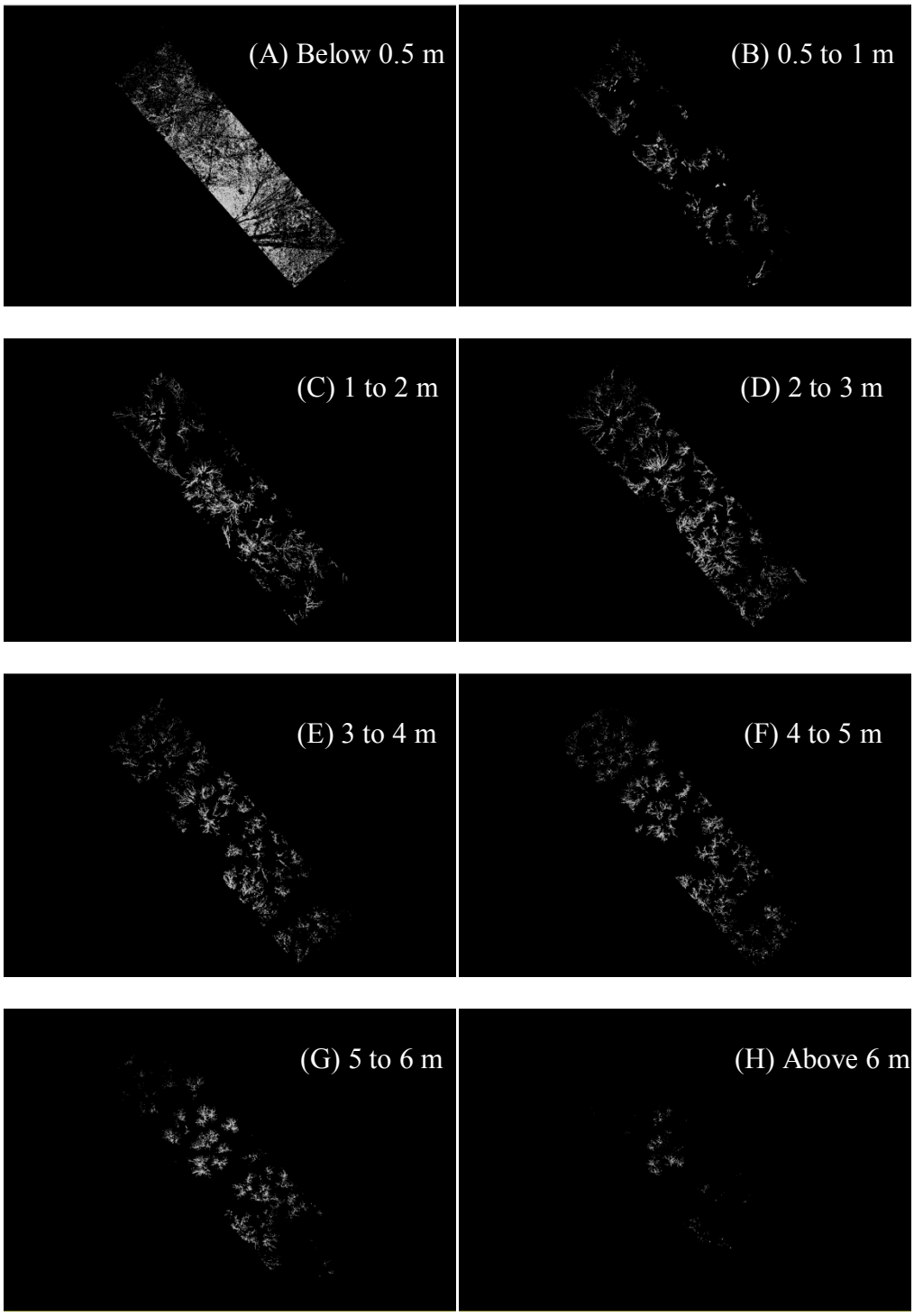

Figure 12. The height bin images of study plot D2.

A stepwise regression was employed to select the appropriate variables for the multiple linear regression model (R. R. Hocking, 1976). The regression analysis used both forward selection and backward elimination to select the best variable combination. The lidar metrics used as independent variables were separated into two groups; one group contained mean height, standard deviation and percentile heights, and the other included normalized height bins. These groups of variables correspond to the two different approaches for analyzing the lidar data.

2.7 Multispectral aerial image classification

Two digital orthophoto quarter quads (DOQQ), Lockett and Boggy Creek, were downloaded from the Texas Natural Resources Information System (TNRIS) and included natural color (blue, green, and red bands) and color-infrared (green, red, and near infrared bands) images. Both images were acquired during leaf-on season in 2008, and cover the Smith Walker Research Unit in Wilbarger County, TX by the USDA National Agriculture Imagery Program (NAIP). The images were resampled from their native resolution of 1 x 1 m to 0.5 x 0.5 m resolution using bicubic spline interpolation and obtained from TNRIS this way. The pair of images for each DOQQ were stacked to create a four-band image including the blue, green, red, and near-infrared bands.

The classification maps were created using the stacked DOQQs with an object-oriented approach implemented the Definiens software. The object-oriented classification algorithm starts with segmentation. Segmentation groups similar,

contiguous pixels into objects based on parameters defined by the user. The multiresolution segmentation algorithm used in Definiens uses parameters, such as scale, color (DN value) vs. shape (complexity), compactness vs. smoothness, and layer weights to determine the homogeneity criteria for creating objects. Parameters were chosen based on multiple trials and personal experience with using DOQQ of similar study areas. Figure 13 (Definiens Developer 7 Reference Book) is a concept flow diagram of the multiresolution segmentation and Table 4 shows the parameters used.

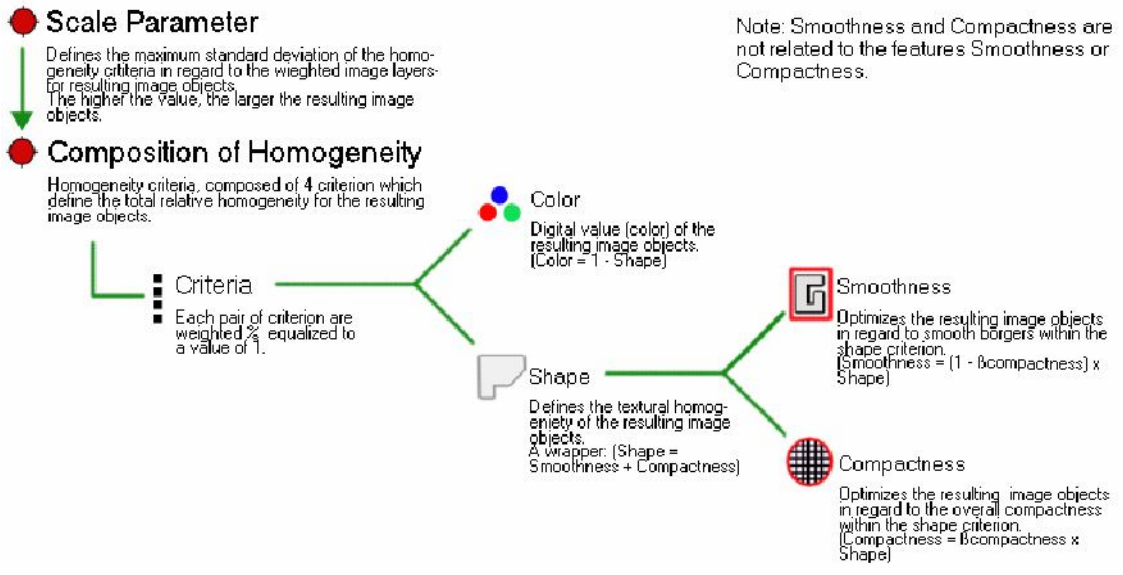

Figure 13. A concept flow diagram of the multiresolution segmentation (Definiens, 2007).

Table 4. The parameters for multiresolution segmentation algorithm

Criteria	Value
Layer Weight	Blue: 1 Green: 1 Red: 1 NIR: 4
Scale Parameter	10
Color vs. Shape	0.9 vs. 0.1
Compactness vs. Smoothness	0.8 vs. 0.2

The final classes in the classification map were (1) mesquite trees, (2) grass, and (3) non-vegetation. The two final classification maps were mosaicked to create one map (Figure 14). The accuracy assessment was conducted by manually assigning a class to each of the 159 randomly selected points (53 per class) when overlaid on the DOQQ The accuracy assessment showed an overall accuracy of 91.20% and kappa coefficient of 0.87, with a kappa coefficient greater than 0.8 representing strong agreement between the classification map and ground points (Jensen, 2005). The classification map was used to mask the non-vegetation pixels from the NDVI map derived in the next step.

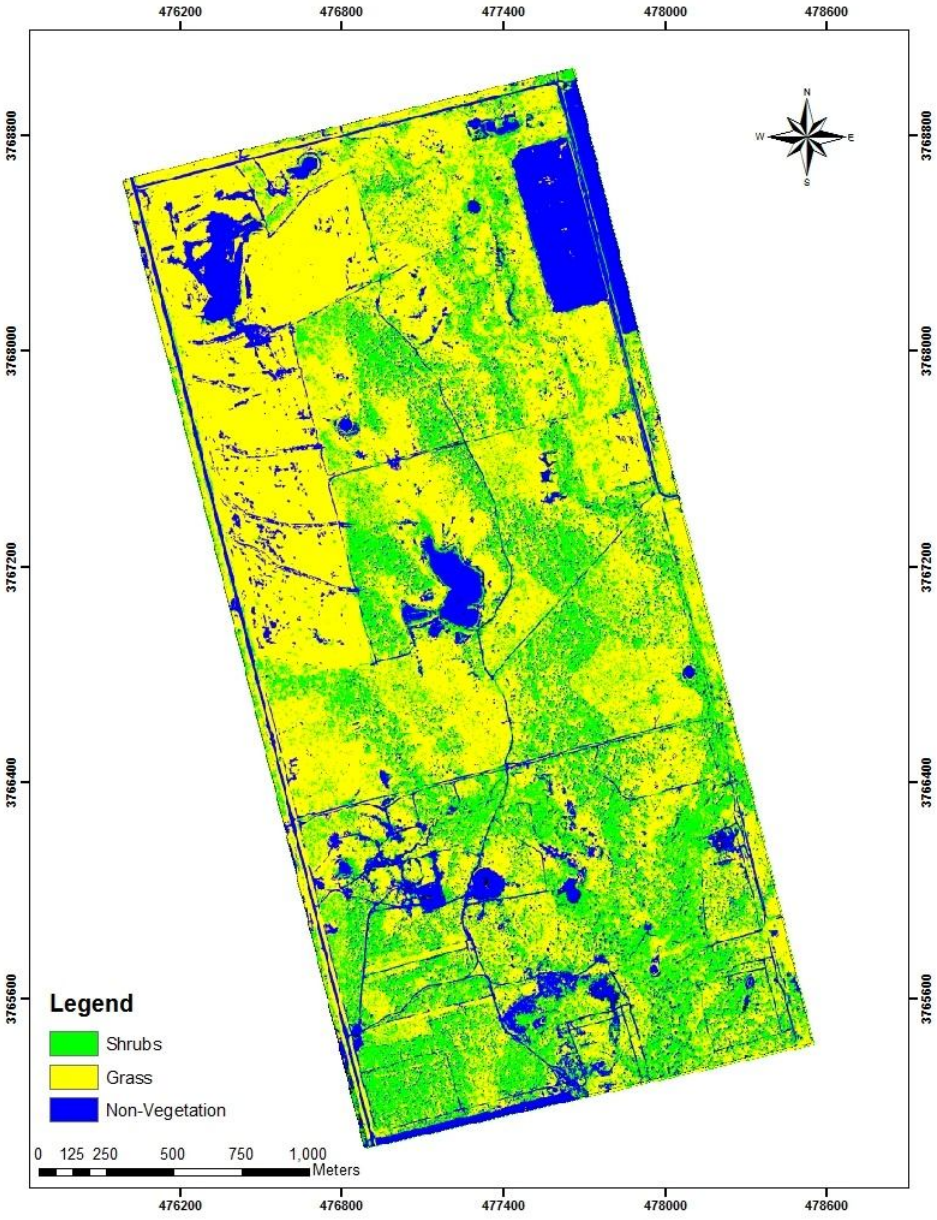

Figure 14. Classification map of Smith Walker Research Unit.

2.8 Normalized difference vegetation index

Vegetation indices are recognized as important vegetation biophysical indicators extracted and modeled using remotely sensed data (Jensen, 2007). A vegetation index should maximize sensitivity to plant biophysical parameters, normalize the model's external effects and the atmosphere, normalize internal effects and differences in senesced or woody vegetation, and be coupled to some specific measurable biophysical parameter. In particular, the Normalized difference vegetation index (NDVI) is broadly applied as an indicator of vegetation "greenness" and is highly correlated with green biomass (Anderson et al. 1993). The following equation shows the NDVI calculation:

$$NDVI = (NIR-Red)/(NIR+Red) \quad \text{(eq. 2)}$$

NIR: Near Infrared band

Red: Red band

2.9 Generating a biomass map

The color-infrared DOQQs were used to generate the NDVI map of the study

area (Figure 15) using equation 2. The classification map was then used to mask out the non-mesquite pixels. Excluding two regrowth plots, 23 individual plot NDVI maps were extracted from the NDVI map of the entire Smith Walker Research Unit. Next, the reference biomass data were converted to geolocated point data based on 98, manually selected, mesquite tree pixels to be used as training points. The reference biomass for each plot was divided by the number of pixels classified as mesquite trees within that plot to calculate each mesquite pixel average biomass. Three to four training points were manually selected from each plot to build the cokriging model. Moran's I, a measure of spatial autocorrelation, indicated spatial autocorrelation with an index of 0.68. Values of Moran's I range from -1 (perfect dispersion) to 1 (perfect correlation) and zero value indicates a random spatial pattern. The NDVI pixels corresponding to the 98 training points were extracted from the plot-level NDVI map. Finally, the corresponding NDVI pixel and training point pairs were used in the cokriging interpolation procedure to generate a biomass prediction map at a local scale.

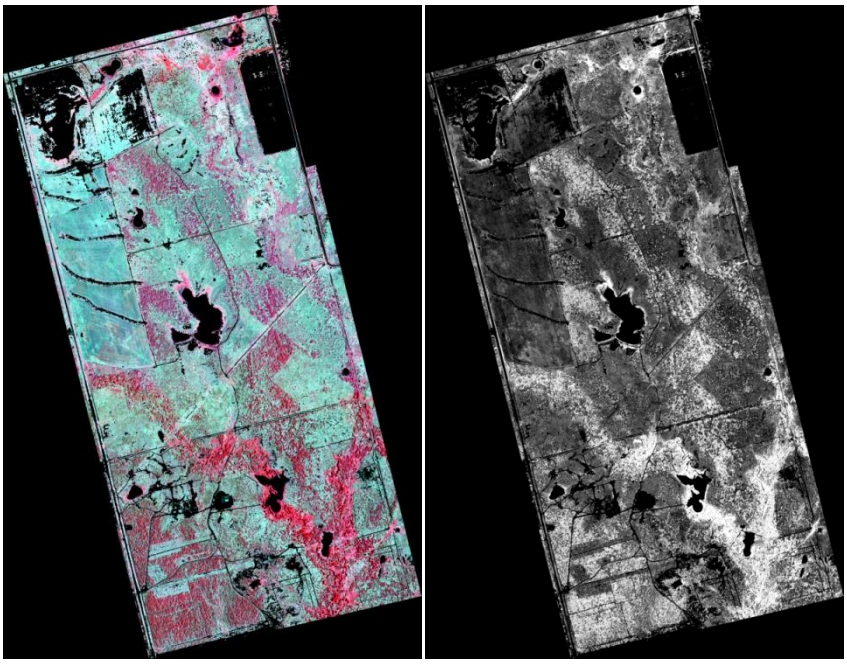

(A) (B)

Figure 15. The preprocessing data for generating a biomass map (A) Color-Infrared vegetation imagery of Smith Walker Research Unit. The black areas are non-vegetation. (B) Vegetation NDVI map. The darker pixels represent low NDVI values and lighter pixels represent high NDVI values.

Cokriging is one member of the kriging family of interpolation methods and allows two variables to be processed together. The accuracy of cokriging predictions is better than other kriging interpolation methods when the two variables have a strong relationship. With a documented relationship between vegetation biomass and NDVI (Anderson et al. 1993), cokriging is appropriate for generating a biomass map. The following is the ordinary cokriging model:

$$\begin{cases} Z_1(s) = \mu_1 + \varepsilon_1(s) \\ Z_2(s) = \mu_2 + \varepsilon_2(s) \end{cases} \quad \text{(eq.3)}$$

Where μ_1 and μ_2 are unknown constants. The $Z_1(s)$ is the biomass data of interest and the $Z_2(s)$ is the NDVI value. The $\varepsilon_1(s)$ and $\varepsilon_2(s)$ are random error parameters. $Z_1(s)$ leverages information from the $Z_2(s)$ variable to help make predictions.

3. RESULTS

3.1 The relationship between terrestrial lidar data and reference biomass

3.1.1 Mean height, standard deviation and percentile heights

Figure 16 shows the regression plots of reference biomass, mean height, standard deviation, and percentile heights, respectively. The relationship between lidar metrics and the reference biomass was nonlinear. Thus, a natural logarithm transformation was employed to transform the reference biomass and the result is shown in figure 17.

The transformation improved R-squared values, indicating a stronger relationship between the individual lidar metrics and the reference biomass data. In addition, the transfomation leads to a linear relationship between the individual lidar metrics and the reference biomass data. Figure 17 shows that the natural logarithm of biomass has a linear relationship with the point cloud height variables.

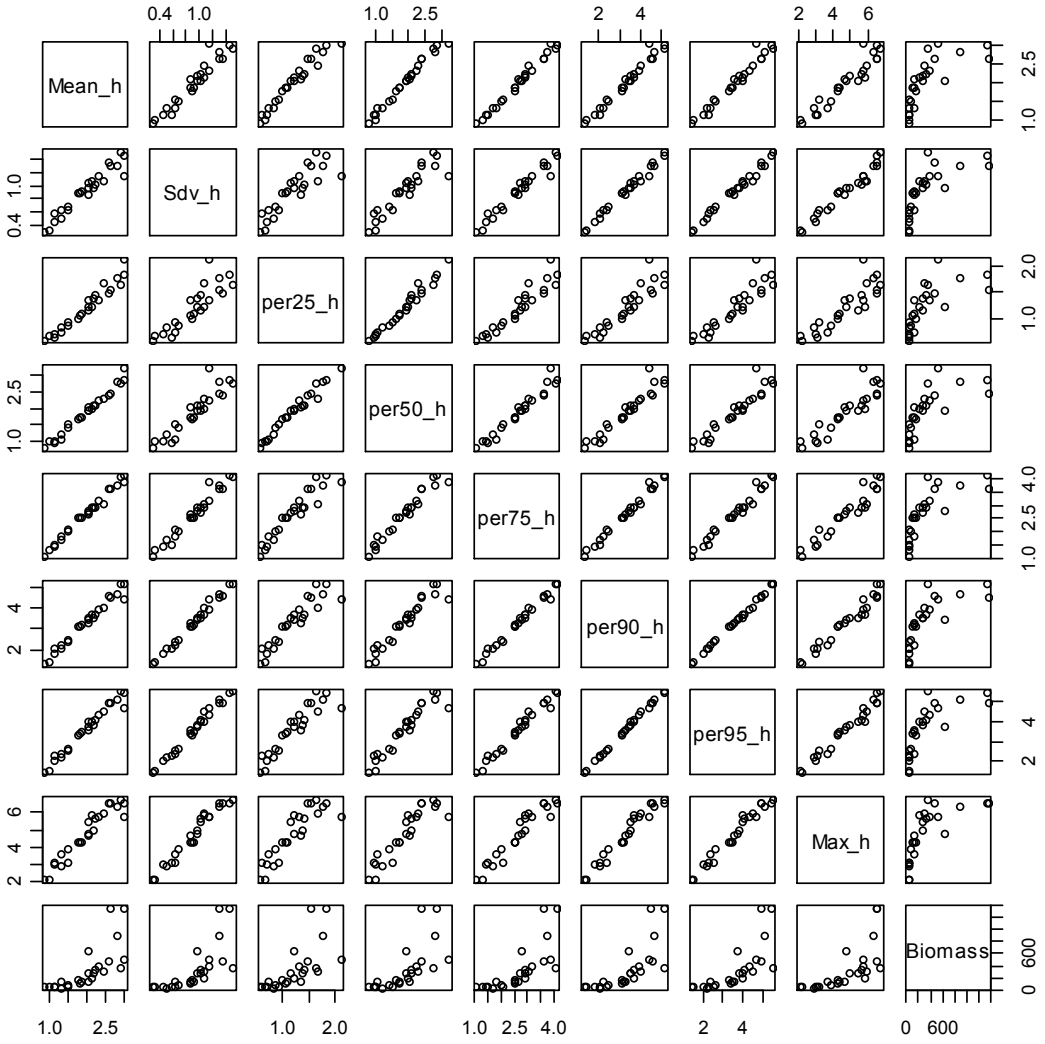

Figure 16. Scatter plots of ground biomass data and the first group of lidar metrics. The points represent each study plot.

Figure 17. Scatter plots of logarithm transformation biomass and the first group of lidar metrics. The points represent each study plot.

Because a high level of correlation between the percentile height variables existed (Figure 17), each variable was used as a simple independent variable and the natural logarithm of the reference biomass data is the dependent variable. The multiple

R-squared and adjusted R-squared values ranged from 0.73 to 0.82 and 0.71 to 0.81, respectively. The high R-squared values indicated that the lidar metrics had high correlation with the natural logarithm of reference biomass. The results show that the reference biomass can be predicted using lidar metrics derived from terrestrial lidar point cloud data.

Table 5. The multiple and adjusted R-square value for each simple linear regression model using the natural logarithm transformation in reference biomass

Point cloud height	Multiple R^2	Adjusted R^2
25th percentile	0.73	0.71
50th percentile	0.75	0.74
75th percentile	0.81	0.80
90th percentile	0.82	0.81
95th percentile	0.82	0.81
Max	0.81	0.80
Mean	0.80	0.79
Standard deviation	0.80	0.80

Although the 90th and 95th height percentiles tied for the highest R-squared values among the group in table 5, the 95th percentile was chosen to be the individual variable to estimate biomass. Therefore, the relationship between the 95th height percentile and the nature logarithms of the reference biomass was used to develop an equation for biomass estimation, as follows:

$$\hat{Y}=100\times\exp(2.34 + 0.81\text{per95\_h} + 1.12) \quad \text{(eq. 4)}$$

Where the first constant,100, extrapolates the biomass estimation from plot level to hectare level. $\hat{Y}$ is the total biomass (kg/ha) and the last constant is the correction factor needed to counteract the systematic bias introduced by the logarithmic transformation (Finney 1941; Baskerville 1972; Sprugel, 1983).

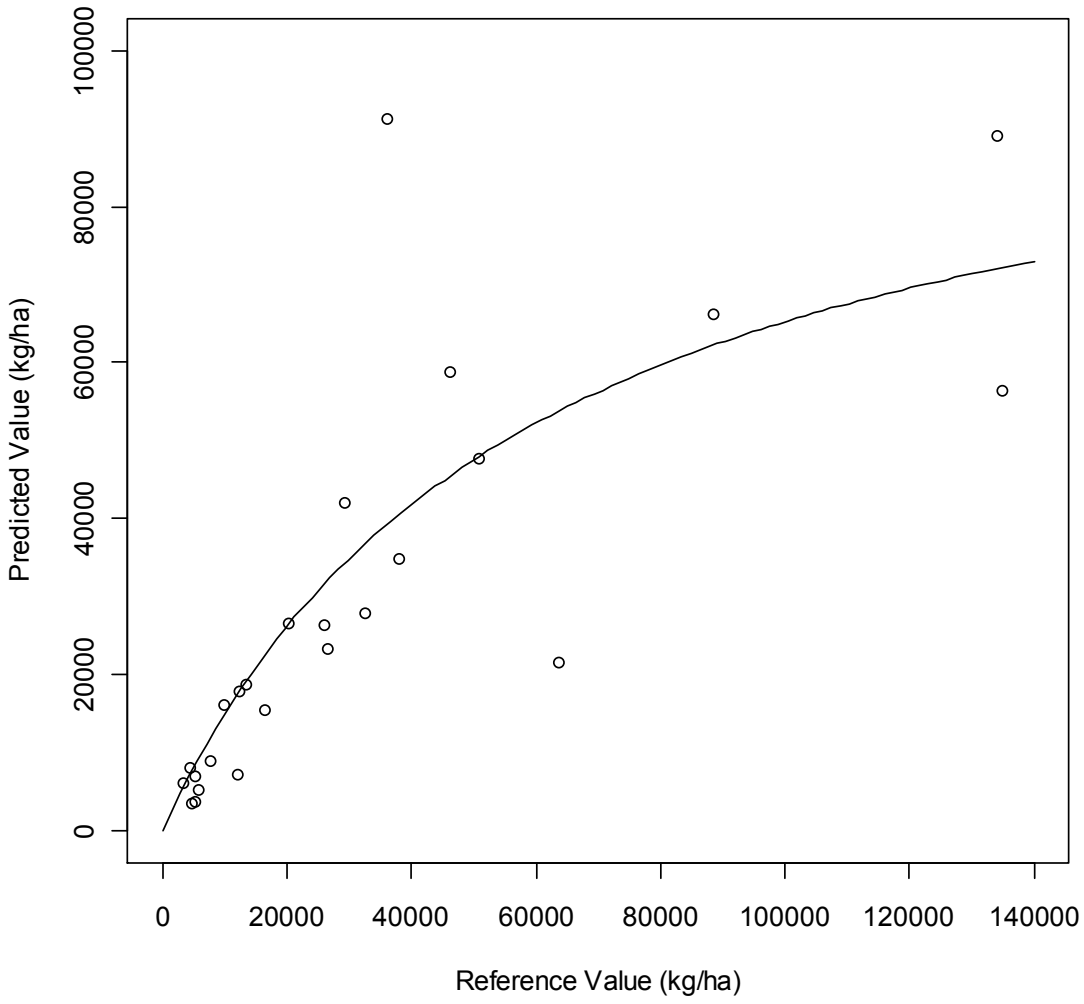

Figure 18. The relationship between ground biomass data and the predicted biomass of point cloud height. The predicted biomass was calculated using equation 3.

3.1.2 Normalized height bins

The second group of lidar metrics includes the normalized height bins. Figure 19 shows a nonlinear relationship in the scatter plots of reference biomass versus normalized height bins. The plots showed the data distributed along a curve with variability increasing as biomass increases. Thus, a natural logarithm transformation was used to transfer the reference biomass and the result is shown in Figure 20.

The logarithmic transformation resulted in improved R-squared values, and indicated that some of the normalized height bins were correlated to the reference biomass data. NHbin1 and NHbin2 have a negative correlation with the natural logarithm of ground biomass data. NHbin3 has a weak relationship with the ground biomass data, but NHbin4 and NHbin5 showed positive correlation. NHbin6 and NHbin7 had many pixels with a zero value, so they were not considered in the regression models. Intially, NHbin1, NHbin2, NHbin4 and NHbin5 were chosen as the independent variables in the height bin model by analyzing the plots of variables against biomass.

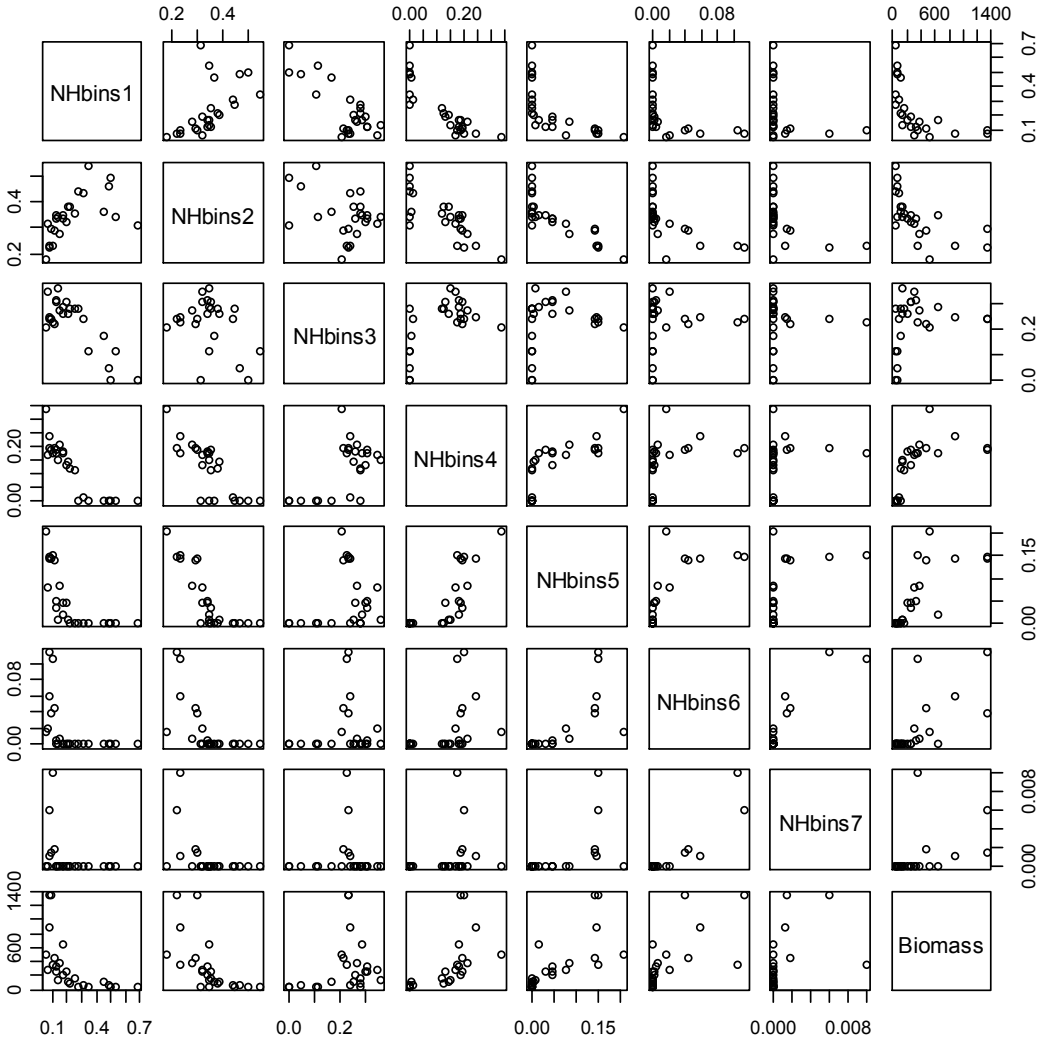

Figure 19. Scatter plots of ground biomass data and the second group lidar metrics. The point represents each study plot.

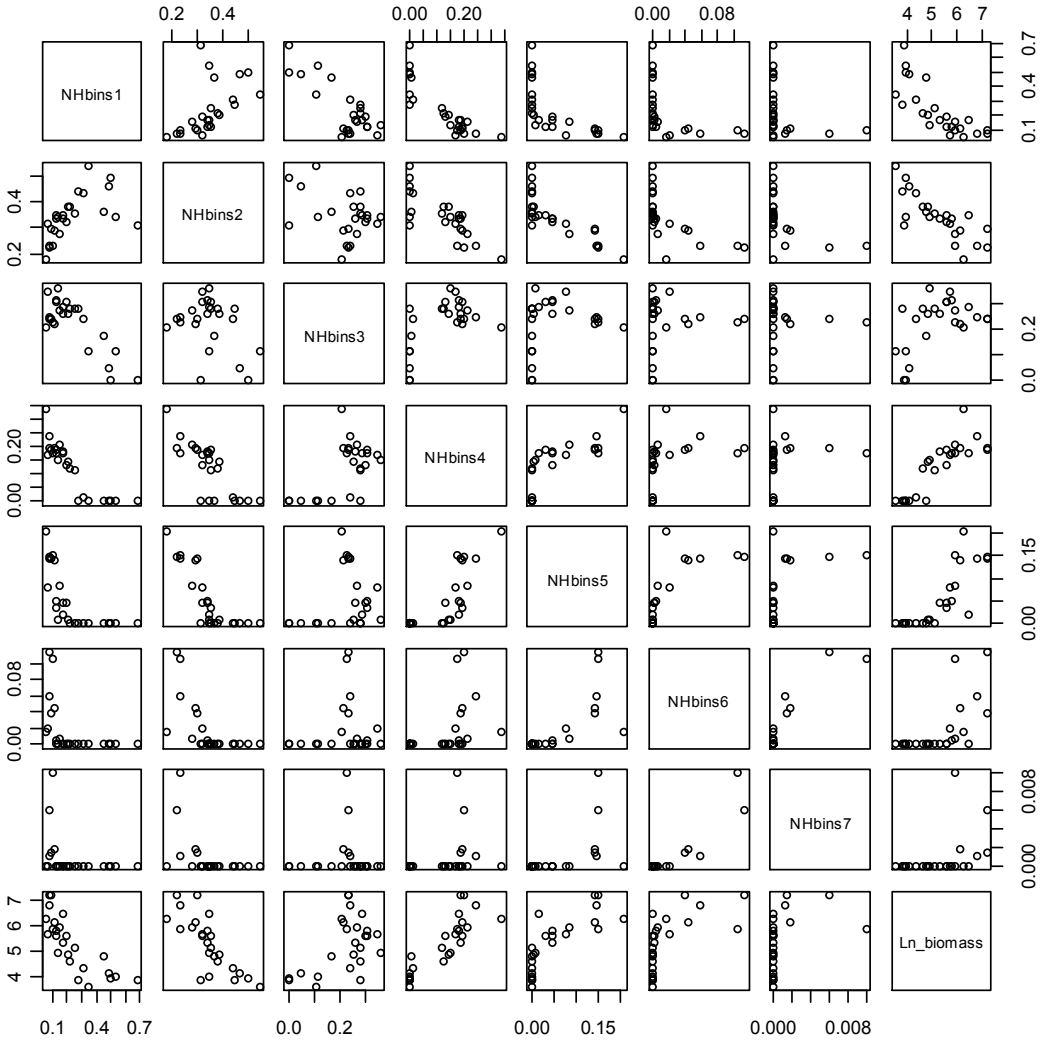

Figure 20. Scatter plots of logarithm transformation biomass and the second group of lidar metrics. The point represents each study plot.

Next, the variables used in the height bin model were narrowed through stepwise regression to find the best variable combination. The variance inflation factor (VIF) was used to examine the height bin variables in the final model to detect possible

multicollinearity effects. Multicollinearity effects appear when two or more variables of the multiple regression model have a strong correlation with each other. The final model (eq. 5) showed no multicolinearity using NHBin1 and NHBin2, as indicated by the VIF for each variable being less than 5.

NHbin1 and NHbin2 are the independent variables in the final height bin model and the natural logarithm of ground biomass data is the dependent variable. The model is given below.

$$\hat{Y}=100\times\exp(8.18 - 3.18NHbin1 - 6.29NHbin2 + 1.14) \quad \text{(eq. 5)}$$

Where the first constant,100, extrapolates the biomass estimation from plot level to hectare level, $\hat{Y}$ is the total biomass (kg/ha), and the last constant item is the correction factor mentioned in the previous paragraph. The multiple R-squared value of the equation was 0.79 and the adjusted R-squared value was 0.77. The final height bin model indicates that the information between 0.5 to 2 m is the most useful for estimating mesquite tree biomass.

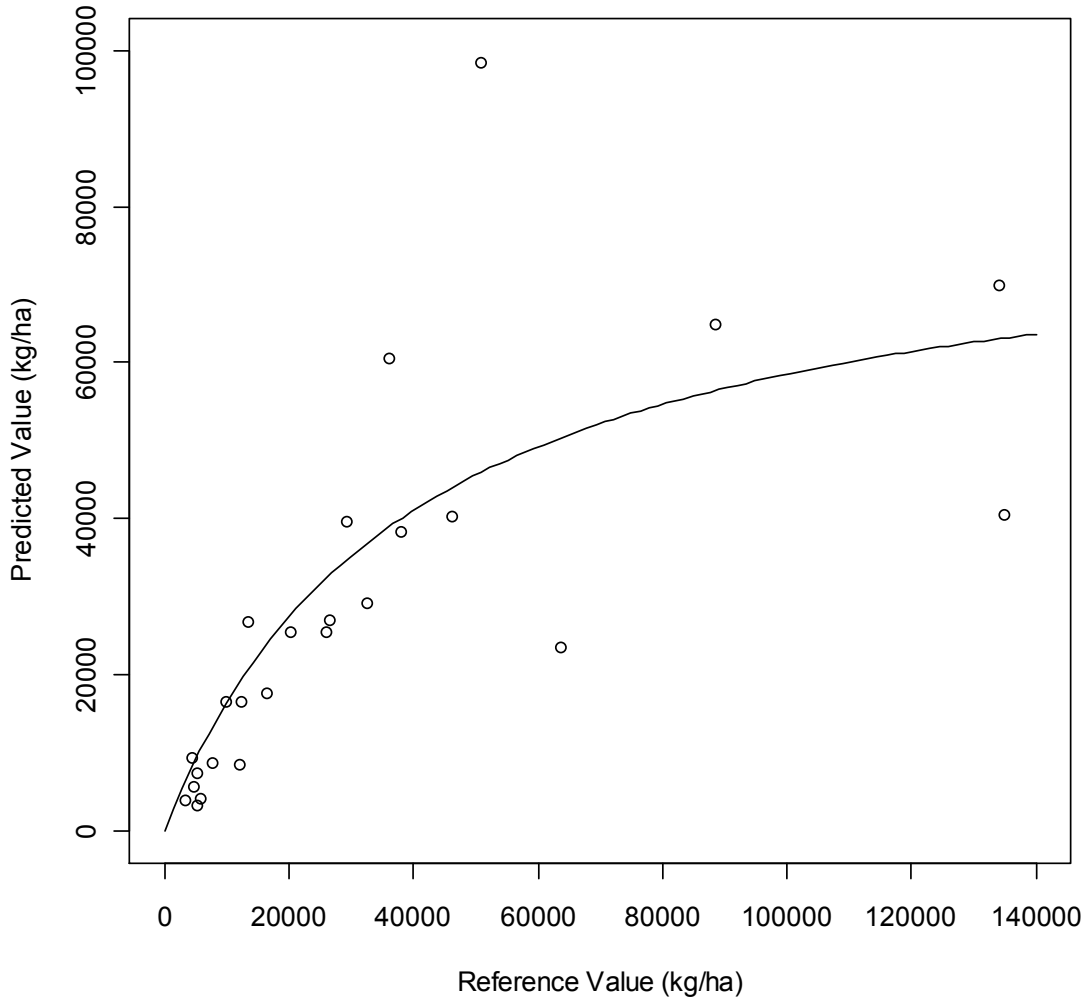

Figure 21. The relationship between ground biomass data and the predicted biomass of height bins. The predicted biomass was calculated using (eq.5).

3.2 Local scale biomass map

The model of ordinary cokriging was determined by the covariance spherical model (Figure 22). The major range was 256.74 m, the lag size was 29.25 m, the partial sill was 14437 and the number of lags was 12. After the model of ordinary cokriging was determined, cross-validation was used to diagnose the model and found its associated parameter values to be reasonable, as shown in figure 23. Cross-validation removes one data location at a time and predicts the associated data value and compares the measured and predicted value. The multiple and adjusted R-squared values were both 0.99 and the root mean square error (RMSE) was 8.3 (kg/ha). The cross-validation results show the cokriging model to be reasonable for generating a biomass map.

The biomass map is shown in Figure 24. The values of mesquite standing biomass in the map represent the biomass of mesquite standing per pixel, with the pixel size being 0.25 m^2. The green color indicates higher biomass, and the red color shows pixels with less biomass values. The biomass map indicates a decreasing biomass gradient in the North-South direction. The reason is that the plots in the northern part of the research unit have larger trees, while the southern part has younger trees.

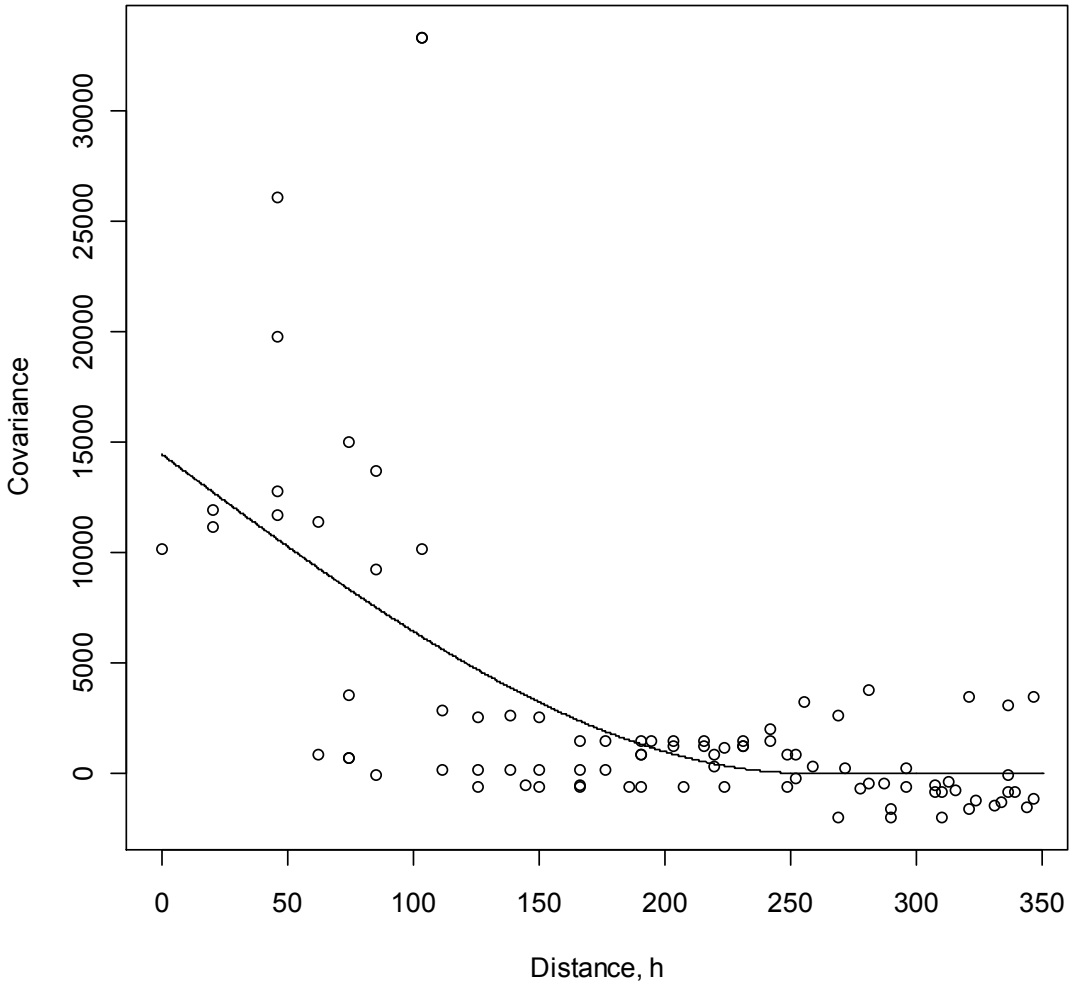

Figure 22. The model of ordinary cokriging –covariance spherical model. The points represent the training points.

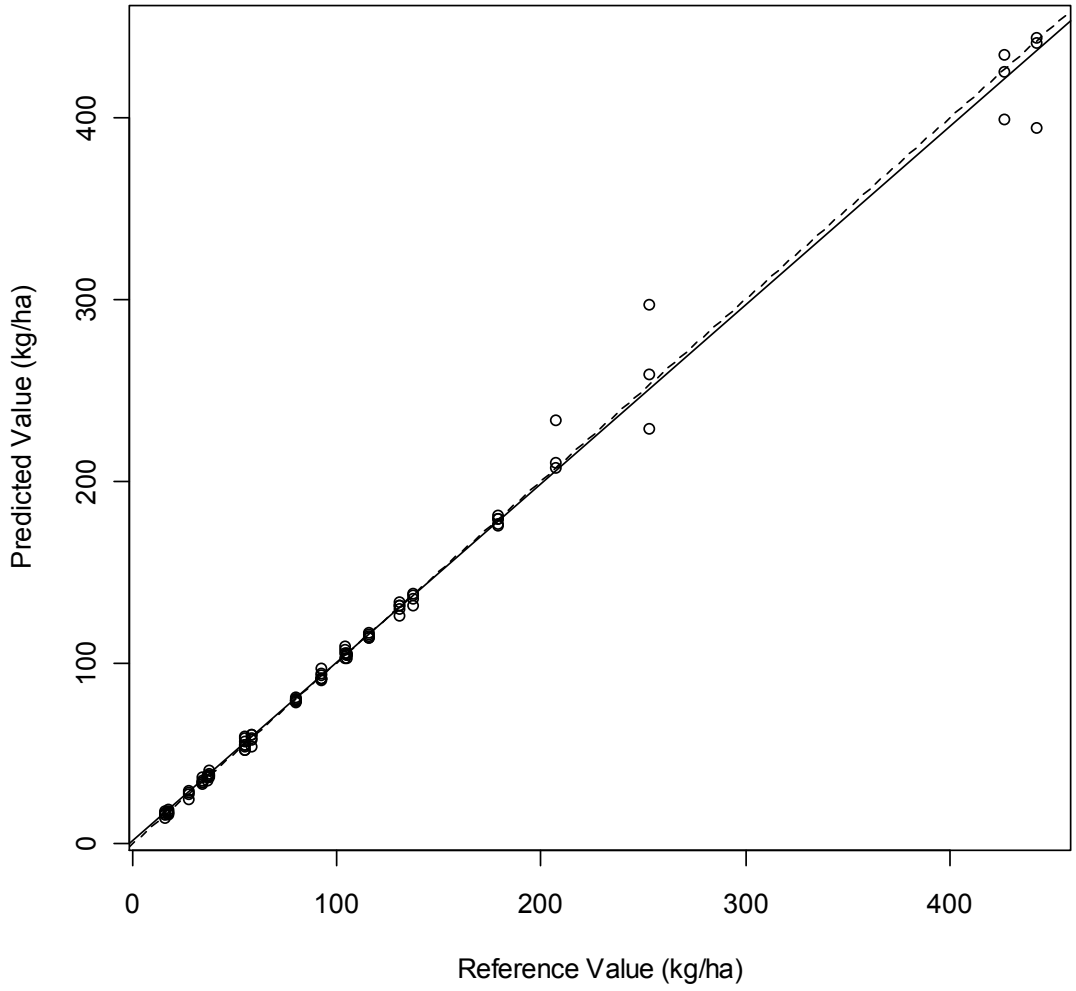

Figure 23. The cross-validation results of ground biomass data (reference value) and predicted biomass (predicted value) using ordinary cokriging to estimate mesquite biomass. The points represent the training points. The solid line is the fitted line and the dashed line shows a one-to-one relationship.

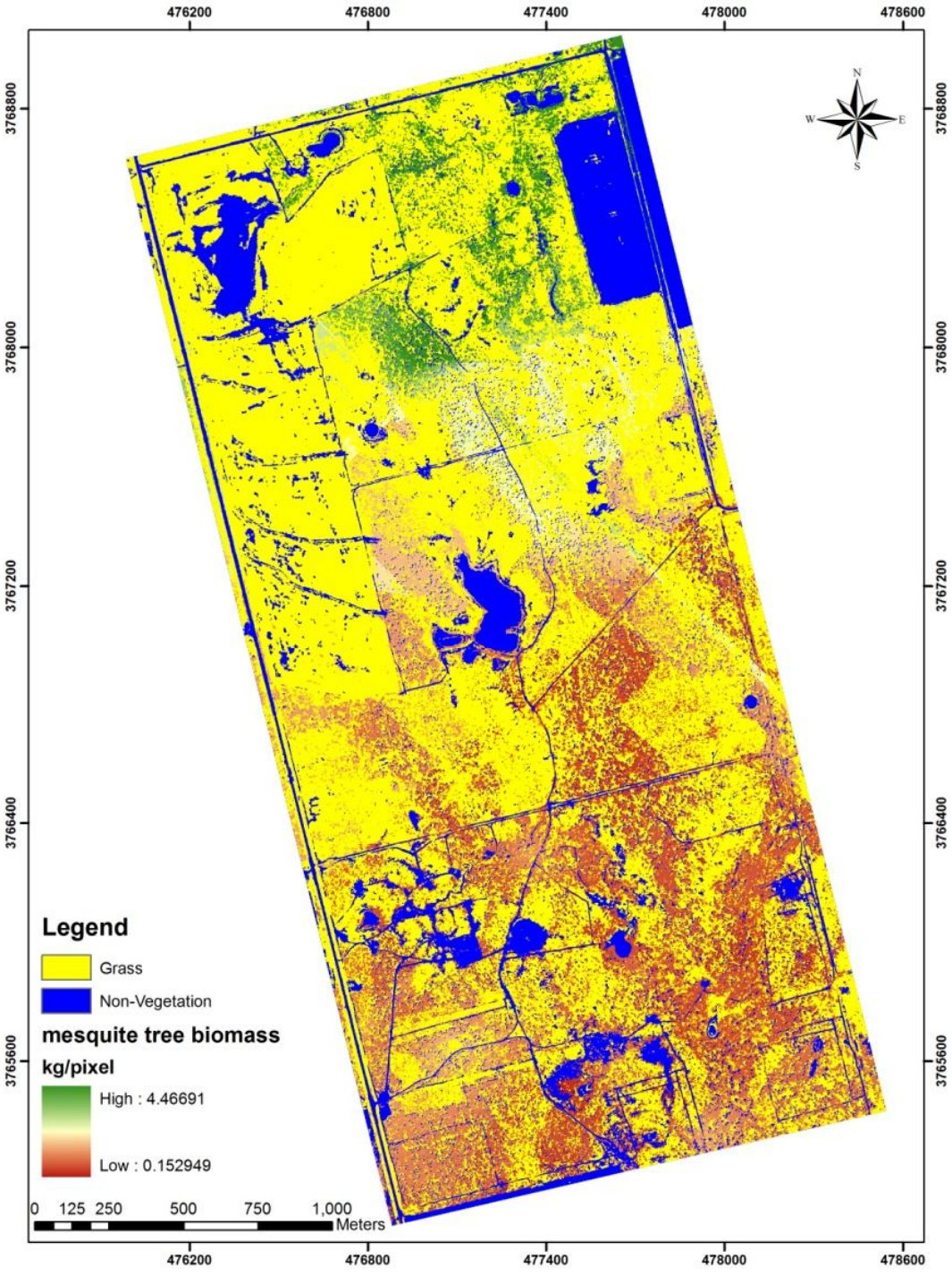

Figure 24. The result of biomass map was created by ordinary cokriging at Smith Walker Research Unit.

4. DISCUSSION

In a forest, the individual tree and forest structures could be accurately derived by terrestrial lidar (Zande et al., 2006; Strahler et al., 2008). However, while we acquired the terrestrial lidar over woody plant vegetation, the individual tree structures were difficult to characterize. The multiple stem mesquite trees had short trunks that made individual stem identification and DBH or stem diameter measurements difficult to estimate using terrestrial lidar data. The terrestrial lidar was able to capture the complex architecture of branches and stems of the mesquite trees. Therefore, we investigated the usefulness of variables derived from lidar point cloud data as independent variables for our biomass estimation equations.

Mesquite tree biomass has been estimated by measuring basal stem diameter and tree height (Felker et al., 1982; Northup et al. 2005; Ansley et al. 2010). Linear regression using woody plant metrics, basal stem diameter and tree height, as independent variables has been used to estimate the green weight of woody plants as well as oven dried biomass. Felker et al. (1982) found the natural logarithm of basal area and stem diameter had high R-squared values (0.9) when compared to the natural logarithm of green weight. Northup et al. (2005) and Ansley et al. (2010) found the relationship between basal stem diameter and oven dried biomass had high correlation, with R-squared values of 0.95 and 0.92, respectively. These results show that basal stem diameter can be a good predictor for estimating both fresh and oven dried biomass. In

our study, the height percentile approach had an R-squared value of 0.81 and the height bins approach had an R-squared value of 0.77 for oven dried biomass.

The comparison of the height percentile and height bins approaches showed the height percentile approach to have a stronger relationship with the woody plant biomass than the height bins approach at plot level, as indicated by the higher R-squared. However, the result of the height bins approach can be more easily interpreted than the height percentiles approach, because height bins have fixed dimensions where height percentiles can vary in the vertical dimension among plots. The height bins model used the lower height bins (NHBin1 and NHBin2) because every plot contained trees at least that tall, whereas not all plots had trees tall enough to have values in the upper height bins (NHBin5, NHBin6 and NHBin7).

NDVI is a modified Simple Ratio Vegetation Index (SR) used to represent the reflectance of near infrared energy, with healthy vegetation having higher NDVI values. In this study, the assumption that the NDVI and reference biomass data would be highly correlated was investigated but found to be weak. The reason could be that although NDVI has been used to estimate vegetation biomass, only one vegetation index may not be enough to accurately predict vegetation biomass. Foody et al. (2003) used more than one hundred LandSat TM band ratios to estimate the correlation between band ratios and biomass. Todd et al. (1998) also used green vegetation index, bright index, wetness index and NDVI to estimate vegetation biomass. In our study, we only investigated NDVI with ground biomass data to create a biomass map. The training points showed strong spatial autocorrelation (Moran's I = 0.68) because the plots were only 100 m² and

a multiple training points had to be selected from each plot to have enough training points to have a large enough sample size to get significant results. Selecting only a single point from each of the 23 plots would eliminate the spatial autocorrelation but would not be enough to estimate biomass. Subsequently, we selected three to four points for each plot, which caused the spatial autocorrelation. As seen in Figure 5, some of the study plots were clumped. To reduce the spatial autocorrelation in the future, training plots should be better distributed throughout the Smith Walker Research Unit. However, our results, when shifting the biomass area reporting units from 0.25 m^2 to 1 hectare, agree with other studies. Whisenant and Burzlaff (1978) found the biomass of old-growth mesquite standing was 19.4 Mg ha^{-1} in Texas and Ansley et al. (2010) also indicated the biomass of mesquite standing at a typical tree density of 750 tree ha^{-1} was 22.1 Mg ha^{-1}.

Satellite images with high spatial resolution could also be used instead of the NAIP aerial image, but the images are more expensive. Future work could investigate the use of high resolution satellite imagery for scaling up biomass estimates and ancillary data, such as maps of soil types, slope, and aspect. Maps of biomass availability can also be combined with road maps to estimate the cost effectiveness of harvesting and transporting mesquite trees to biomass plants for bioenergy production.

5. CONCLUSION

The study provides new methodologies for rangeland managers and researchers to estimate the biomass of woody plants at plot level and this non-destructive method may be helpful in quantifying the amount of bioenergy that can be generated by removing woody plants from an area. The height bin model is more easily interpreted than the height percentile model. Although the height percentile model had a higher R-squared value than the height bin model, the independent variables used with the height bin model are robust. Future studies could combine terrestrial and airborne lidar data to improve the height bin model with a data fusion approach. Airborne lidar could provide better point cloud data at the top of the woody plants canopy while terrestrial lidar has the ability to scan lower layers of the canopy.

Multispectral imagery covered a larger area than the terrestrial lidar data. Future studies could focus on the development of methods by using high spatial resolution satellite imagery or airborne lidar data for assessing woody plant biomass at local to regional scales. Furthermore, we need a better distribution of training points to improve our biomass map.

Overall, the study used an emerging lidar technology to assess woody plant biomass and create new equations for estimating woody plant biomass. In addition, the study used NAIP aerial imagery to create a biomass map at a local level.

REFERENCES

Anderson, G. L., Hanson, J. D., & Haas, R. H. (1993). Evaluating Landsat Thematic Mapper derived vegetation indices for estimating above-ground biomass on semiarid rangelands. *Remote Sensing of Environment, 45*, 165–175.

Ansley, R. J., Mirik, M., & Castellano, M. J. (2010). Structural biomass partitioning in regrowth and undisturbed mesquite (*Prosopis glandulosa*): implications for bioenergy uses. *Global Change Biology Bioenergy, 2*, 26-36.

Boelman, N. T., Stieglitz, M., Rueth, H. M., Sommerkorn, M., Griffin, K. L., Shaver, G. R., & Gamon, J. A. (2003). Response of NDVI, biomass, and ecosystem gas exchange to long-term warming and fertilization in wet sedge tundra. *Oecologia 135*(3), 414-421.

Brown, J. R. & Archer, S. (1989). Woody plant invasion of grasslands: establishment of honey mesquite (*Prosopis glandulosa var. glandulosa*) on sites differing in herbaceous biomass and grazing history. *Oecologia, 80*, 19-26.

Chen, Q., Baldocchi, D., Gong, P., & Kelly, M. (2006). Isolating individual trees in a savanna woodland using small footprint lidar data. *Photogrammetric Engineering and Remote Sensing, 72*(8), 923-932.

Chojnacky, D. C. (2002). Allometric scaling theory applied to FIA biomass estimation. In McRoberts RE, Reams GA, Van Deusen PC, Moser JW (Eds.), *Proceedings of*

Third Annual Forest Inventory and Analysis Symposium, 17-19 October 2001, Traverse City, MI. (pp. 96–102) Gen. Tech. Rep. NC-230. St. Paul, MN: U.S. Department of Agriculture, Forest Service, North Central Research Station.

Clayton, M. (2008). As global food costs rise, are biofuels to blame? *Christian Science Monitor*. http://www.csmonitor.com/Money/2008/0128/p03s03-usec.html. last accessed on Apr. 4, 2010.

Davis, Charles G. Vernon, TX. *Handbook of Texas Online.* http://www.tshaonline.org /handbook/online/articles/hev01, accessed November 25, 2010.

Definiens Developer 7 Reference Book. (2007). http://www.pcigeomatics.com/products /pdfs/definiens/ReferenceBook.pdf, accessed on December 21, 2010.

Demirbas, A. (2009). Political, economic and environmental impacts of biofuels: A review. *Applied Energy, 86*, 108-117.

Department of Energy (2010). Fossil Fuels. http://www.energy.gov/energysources /fossilfuels.htm, last accessed on Sept. 02, 2010.

Felker, P. (1984). Economic, environmental, and social advantages of intensively managed short rotation mesquite (*Prosopis* spp) biomass energy farms. *Biomass, 5*, 65-77.

Felker, P., Clark, P. R., Osborn, J. F., & Cannell, G. H. (1981). Screening *Prosopis* (Mesquite or Algarrobo) for biofuel production on semiarid lands. *Symposium on*

Dynamics and Management of Mediterranean-type Ecosystems. June 22-26, 1981, San Diego, CA.

Felker, P., Clark, P. R., Osborn, J. F., & Cannell, G. H. (1982). Biomass estimation in a young stand of mesquite (*Prosopis* spp), ironwood (*Olneya tesota*), Palo Verde (*Cercidium floridium*, and *Parkinsonia aculeata*), and Leucaena (*Leucaena leucocephala*). *Journal of Range Management, 35*(1), 87-89.

Foody, G.M., Boyd, D.S., & Cutler, M.E.J. (2003). Predictive relations of tropical forest biomass from Landsat TM data their transferability between regions. *Remote Sensing of Environment, 85*, 463–474.

Forman, R.T.T. (1995). Some general principles of landscape and regional ecology. *Landscape Ecology, 10*, 133-142

Henning, J. G., & Radtke, P. J. (2006a). Detail stem measurements of standing trees from ground-based scanning lidar. *Forest Science, 52*(1), 67-80.

Henning, J. G., & Radtke, P. J. (2006b). Ground-based laser imaging for assessing three-dimensional forest canopy structure. *Photogrammetric Engineering & Remote Sensing, 72*(12), 1349-1358.

Hierro, J. L., Branch, L. C. Villarreal D., & Clark, K. L. (2000). Predicted equations for biomass and fuel characteristics of Argentine shrubs. *Journal of Range Management, 53*(6), 617-621.

Hopkinson, C., Chasmer, L., Young-Pow , C., & Treitz, P. (2004). Assessing forest metrics with a ground-based scanning lidar. *Canadian Journal of Forest Research. 34*, 573-583.

Jenkins, J. C., Chojnacky, D. C., Heath, L. S., & R. Birdsey, A. (2003). National-scale biomass estimators for United States tree species. *Forest Science, 49*(1), 12-35.

Jensen, John R. (2005*). Introductory digital image processing-A remote sensing perspective.* (3rd ed.). Upper Saddle River, NJ: Pearson Education, Inc.

Jensen, John R. (2007). *Remote sensing of the environment-An earth resource perspective.* (2nd ed.). Upper Saddle River, NJ: Pearson Education, Inc.

Kiniry, J. R., (1998). Biomass accumulation and radiation use efficiency of honey mesquite and eastern red cedar. *Biomass & Bioenergy, 15*(6), 467-473.

Lefsky, M. A., Cohen, W. B., Parker, G. G. & Harding, D. J. (2002). Lidar remote sensing for ecosystem studies. *Bioscience, 52*(1), 19-30.

Lefsky, M. A., Harding, D., Cohen, W. B., Parker, G. & Shugart, H. H. (1999). Surface lidar remote sensing of basal area and biomass in deciduous forests of eastern Maryland, USA. *Remote Sensing of Environment, 67*(1), 83-98.

Little, E.L., Jr. (1976). *Atlas of United States trees, volume 3, minor Western hardwoods:* U.S. Department of Agriculture, Washington, D.C. Miscellaneous Publication No. 1314.

Little, E.L., Jr. (2006). *Field guide to trees-eastern region*. New York: Alfred A. Knopf, Inc.

Maas, H. -G., Bienert, A., Scheller, S., & Keane, E. (2008). Automatic forest inventory parameter determination from terrestrial laser scanner data. *International Journal of Remote Sensing, 29*(5), 1579-1593.

Magnussen, S., & Boudewyn, P. (1998). Derivations of stand heights from airborne laser scanner data with canopy-based quantile estimators. *Canadian Journal of Forest Research. 28,* 1016-1031.

Maltamo, M., Packalen, P., Yu, X., Eerikainen, K., Hyyppa, J., & Pitkanen, J. (2005). Identifying and quantifying structural characteristics of heterogeneous boreal forests using laser scanner data. *Forest Ecology and Management, 216*(1-3), 41-50.

Næsset, E. & Bjerknes, K.-O. (2001). Estimating tree heights and number of stems in young forest stands using airborne laser scanner data. *Remote Sensing of Environment, 78*, 328-340.

Næsset, E. (2004). Practical large-scale forest stand inventory using a small-footprint airborne scanning laser. *Scandinavian Journal of Forest Research, 19*, 164 -179.

Navar, J., Najera J., & Jurado, E. (2002). Biomass estimation equations in the Tamaulipan thornscrub of north-eastern Mexico. *Journal of Arid Environments, 52*(2), 167-179.

Nelson, R., Krabill, W., and Tonelli, J. (1988). Estimating forest biomass and volume using airborne laser data. *Remote Sensing of Environment, 24*(2), 247-267.

Northup, B.K., Zitzer, S.F., Archer, S., McMurtry, C.R., & Boutton, T.W. (2005). Above-ground biomass and carbon and nitrogen content of woody species in a subtropical thornscrub parkland. *Journal of Arid Environments, 62,* 23-43.

Paruelo, J. M., Epstein, H. E., Lauenroth, W. K., & Burke, I. C. (1997). ANPP estimates from NDVI for the central grassland region of the United States. *Ecology, 78*(3), 953–958.

Patenaude, G., Hill, R.A., Milne, R., Gaveau, D.L.A., Briggs, B.B.J., & Dawson, T.P. (2004). Quantifying forest above ground carbon content using LiDAR remote sensing. *Remote Sensing of Environment, 93,* 368-380.

Popescu, S.C. (2007). Estimating biomass of individual pine trees using airborne lidar. *Biomass & Bioenergy, 31*, 646-655.

Popescu, S.C., & Zhao, K. (2008). A voxel-based lidar method for estimating crown base height for deciduous and pine trees. *Remote Sensing of Environment, 112,* 767-781.

Popescu, S.C., Wynne, R.H., & Nelson, R.F. (2003). Measuring individual tree crown diameter with lidar and assessing its influence on estimating forest volume and biomass. *Canadian Journal of Remote Sensing, 29,* 564-577.

Smith, J.E., Heath, L.S., Jenkins, J.C., & United States. Forest Service. Northeastern Research Station. (2003). *Forest volume-to-biomass models and estimates of mass for live and standing dead trees of U.S. forests.* Newton Square, PA: U.S. Dept. of Agriculture, Forest Service, Northeastern Research Station.

Strahler, A.H., Jupp, D. L. B., Woodcock, C.E., Schaaf, C.B., Yao, T., Zhao, F., Yang, X., Lovell, J., Culvenor, D., Newnham, G., Ni-Meister, W. And Boykin-Morris, W. (2008). Retrieval of forest structural parameters using a ground-based lidar instrument (Echidna®). *Canadian Journal of Remote Sensing*, *34*, S426—S440.

Todd, S.W., Hoffer, R.M., & Milchunas, D.G. (1998). Biomass estimation on grazed and ungrazed rangelands using spectral indices. *International Journal of Remote Sensing, 19*, 427–438.

Van Auken, O. W. (2000). Shrub invasions of North American semiarid grasslands. *Annual Review of Ecology and Systematics, 31,* 197-215.

Van der Zande, D., Hoet, W., Jonckheere, L., van Aardt, J., & Coppin, P. (2006). Influence of measurement set-up of ground-based LiDAR for derivation of tree structure. *Agricultural and Forest Meteorology, 141,* 147-160.

Whisenant, S.G., & Burzlaff, D.F. (1978). Predicting green weight of mesquite (*Prosopis glandulosa torr*). *Journal of Range Management*, *31*, 396-397

Zheng, D.L., Rademacher, J., Chen, J.Q., Crow, T., Bresee, M., le Moine, J., & Ryu, S.R. (2004). Estimating aboveground biomass using Landsat 7 ETM+ data across a

managed landscape in northern Wisconsin, USA. *Remote Sensing of Environment, 93*, 402-411

VITA

Name: Nian-Wei Ku

Education: B.S. Forestry-National Chiayi University, Taiwan (ROC)

M.S. Forestry-Texas A&M University, USA

Address: Department of Ecosystem Science and Management,

Spatial Sciences Laboratory,

1500 Research Plaza, Office 217,

College Station, TX 77843-2120, USA

E-mail: goofno17@tamu.edu